



**HAL**  
open science

## Late paleozoic pre and syn-kinematic plutons of the Kangguer-Huangshan shear zone: inference on the tectonic evolution of the eastern Chinese North Tianshan.

Bo Wang, Dominique Cluzel, Bor-Ming Jahn, Liangshu S. Shu, Yan Chen, Yazhong Zhai, Yannick Branquet, Luc Barbanson, Stanislas Sizaret

### ► To cite this version:

Bo Wang, Dominique Cluzel, Bor-Ming Jahn, Liangshu S. Shu, Yan Chen, et al.. Late paleozoic pre and syn-kinematic plutons of the Kangguer-Huangshan shear zone: inference on the tectonic evolution of the eastern Chinese North Tianshan.. American journal of science, 2014, 314, pp.43-79. 10.2475/01.2014.02 . insu-00966704

**HAL Id: insu-00966704**

**<https://insu.hal.science/insu-00966704>**

Submitted on 7 Jun 2023

**HAL** is a multi-disciplinary open access archive for the deposit and dissemination of scientific research documents, whether they are published or not. The documents may come from teaching and research institutions in France or abroad, or from public or private research centers.

L'archive ouverte pluridisciplinaire **HAL**, est destinée au dépôt et à la diffusion de documents scientifiques de niveau recherche, publiés ou non, émanant des établissements d'enseignement et de recherche français ou étrangers, des laboratoires publics ou privés.

# LATE PALEOZOIC PRE- AND SYN-KINEMATIC PLUTONS OF THE KANGGUER–HUANGSHAN SHEAR ZONE: INFERENCE ON THE TECTONIC EVOLUTION OF THE EASTERN CHINESE NORTH TIANSHAN

BO WANG\*<sup>†</sup>, DOMINIQUE CLUZEL\*\*, BOR-MING JAHN\*\*\*, LIANGSHU SHU\*,  
YAN CHEN<sup>§</sup>, YAZHONG ZHAI\*, YANNICK BRANQUET<sup>§</sup>, LUC BARBANSO<sup>§</sup>,  
and STANISLAS SIZARET<sup>§</sup>

**ABSTRACT.** Permian large-scale transcurrent tectonics and massive magmatism are prominent features of the Tianshan belt and neighboring regions of the Central Asian Orogenic Belt. Structural, geochronological and geochemical analyses of Carboniferous and Permian intrusive rocks associated with the Kangguer–Huangshan Shear Zone (eastern Chinese North Tianshan) provide constraints on their tectonic setting and the tectonic evolution of the Tianshan belt as well. Carboniferous granitic rocks were emplaced at  $338 \pm 4$  Ma and  $347 \pm 2$  Ma, respectively, and show geochemical features typical of the calc-alkaline series. These arc-type granites do not display ductile deformation, probably because they were completely cooled at the time of shearing tectonics, and are only offset by brittle strike-slip faults. In contrast, Permian granitoids display pervasive ductile tectonic features diagnostic of synkinematic emplacement.

Four gabbro and diorite samples from the East Huangshan intrusive complex yielded zircon U-Pb ages of 267 to 275 Ma, and a granitic dike is dated at  $290 \pm 1$  Ma. The granitic dike is cut by en-echelon right-lateral strike-slip faults, and the mafic intrusive complex displays a sigmoidal shape with mylonitic foliation localized at its margins. Other specific pluton shapes (such as tongue and tadpole-like) and syn-magmatic deformation can be observed in intrusions of the same age, showing similar fabrics and kinematics consistent with that of the Kangguer–Huangshan Shear Zone. Numerous mafic to felsic dikes occur within and off the shear zone with a dominant SE-NW orientation and minor varieties in N-S or NNE-SSW directions. One gabbro dike that intrudes the early Carboniferous granite of the East Kanggurtag area yielded a magmatic age of  $274 \pm 4$  Ma, and contains older zircons ( $\sim 340$  Ma,  $\sim 390$  Ma,  $\sim 450$  Ma, and 1.3–2.2 Ga) probably inherited from intruded rocks. The Permian intrusive rocks have variable chemical compositions suggesting derivation of these rocks from depleted and undepleted (or enriched) mantle sources with involvement of subduction-related components. We conclude from our integrated analysis of the geological, structural, geochemical and geochronological data that the Permian magmatic rocks were formed in a post-collisional/post-orogenic setting from multiple sources, and were emplaced under the control of large-scale dextral transcurrent tectonics.

Key words: Late Paleozoic, Permian, Central Asia, Tianshan, Kangguer–Huangshan shear zone, post-collision, synkinematic magmatism, transcurrent tectonics

## INTRODUCTION

The Permian is a critical period in the building of the Central Asian Orogenic Belt (CAOB) and its amalgamation with the Tarim-Sino Korean (North China) plates in

\* State Key Laboratory for Mineral Deposits Research, School of Earth Sciences and Engineering, Nanjing University, Nanjing 210093, China

\*\* Pôle Pluri-disciplinaire de la Matière et de l'Environnement-EA 3325, Université de la Nouvelle-Calédonie, BP R4, 98851 Noumea cedex, New Caledonia

\*\*\* Department of Geological Sciences, National Taiwan University, Taipei, 10617

§ Institut des Sciences de la Terre d'Orléans, UMR 7427–CNRS/Université d'Orléans/BRGM, 1A, rue de la Férollerie, 45071 Orléans cedex 2, France

† Corresponding author: B. Wang bwang@nju.edu.cn; phone: +86-25-8359-2921

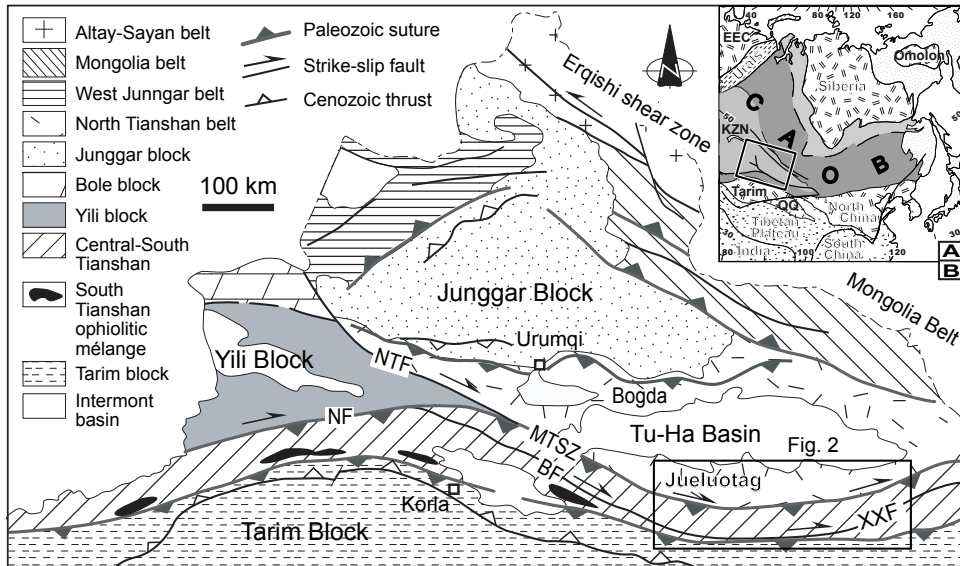


Fig. 1. (A) Simplified tectonic map of eastern Eurasia (modified after Jahn, 2004). Abbreviations for tectonic units: CAOB, Central Asian Orogenic Belt; EEC, East European Craton; KZN, Kazakhstan; QQ, Qaidam Qiling. (B) Sketch map of the northern Xinjiang area, NW China, showing tectonic subdivisions of the Chinese Tianshan and main bounding faults (modified from Wang and others, 2007). Abbreviations: NTF, North Tianshan Fault; NF, Nalati Fault; MTSZ, Main Tianshan Shear Zone; BF, Baluntai Fault; XXF, Xingxingxia Fault.

the south and the Siberian Craton in the north (fig. 1A) (Jahn and others, 2000a, 2000b; Jahn, 2004; Kröner and others, 2007; Windley and others, 2007; Xiao and others, 2009a, 2009b, 2010a). Large volumes of Permian magmatic rocks are spread throughout the CAOB, and significantly contributed to the Phanerozoic continental growth by the input of mantle-derived material (Jahn, 2004; Jahn and others, 2009). The tectonic setting of the magmatic rocks is a key point for deciphering the geodynamic evolution of the CAOB.

The Tianshan Belt is located in the southernmost part of the CAOB and is important for the understanding of the welding of Tarim with the CAOB (Charvet and others, 2007, 2011). The Tianshan belt is generally considered to have formed in Paleozoic time, but the timing of final amalgamation is variously proposed as (1) pre-Carboniferous (Xia and others, 2004, 2008), (2) Carboniferous to early Permian (Coleman, 1989; Allen and others, 1993; Gao and others, 1998, 2009; Chen and others, 1999; Heubeck, 2001; Shu and others, 2000, 2004; Wang and others, 2008a, 2010, 2011; Hegner and others, 2010; Han and others, 2011), and (3) Permian to Triassic (Xiao and others, 2004, 2009a, 2009b, 2010a; Zhang and others, 2007).

It is clear that the controversies focus on the tectonic significance of the Permian geological events. One way to test different models is to verify the tectonic setting(s) of the Permian magmatic rocks, which are widely distributed in the Chinese Tianshan and have been well investigated by previous authors. However, there is still a hot debate on the tectonic setting of the Permian magmatic rocks, and diverse models include (1) post-collisional (Li and others, 2006b; Wang and others, 2008b; Tang and others, 2008), (2) continental rifting (Che and others, 1996; Shu and others, 2011), (3) island arc (Mao and others, 2006), and (4) super mantle plume-related Large Igneous Province (Xia and others, 2004, 2008; Su and others, 2011). These contrasting

interpretations were proposed for one single region and one single period (Permian), and cannot all be correct. Further comprehensive studies of Permian magmatic rocks and their tectonic environment are thus necessary.

In addition, Permian large-scale strike-slip faults or shear zones are a prominent tectonic feature of the CAOBS and play an essential role in the formation of the present structure of the region (Şengör and others, 1993; Allen and others, 1995; Şengör and Natal'in, 1996; Wang and others, 2006a, 2010, 2011; Buslov, 2011). Shear-induced transtension and/or localized failure favor ascent and emplacement of magma (Lees, 2002; Weinberg and others, 2004) and can be used to interpret magmatic rocks in an orogenic belt or a post-collisional belt (Liegeois, 1998; Wang and others, 2009; Litvinovsky and others, 2011). In the Chinese Tianshan, several mega-shear zones occur sub-parallel to the belt (Yin and Nie, 1996; Shu and others, 1999; Laurent-Charvet and others, 2002, 2003; Wang and others, 2006a, 2008c, 2010), but only a few studies have invoked the role of large-scale shear zones in the emplacement of synkinematic plutons (Wang and others, 2009; Pirajno, 2010; Branquet and others, 2012).

In order to better understand the tectonic setting(s) of the Permian magmatic rocks and to place more constraints on the tectonic evolution of the Tianshan belt, we studied the structural features of Permian intrusions within the Kangguer–Huangshan shear zone, eastern Chinese North Tianshan. We also present new zircon U-Pb ages and whole-rock geochemical data for these intrusive rocks. Early Carboniferous pre-kinematic granitic rocks were also investigated, and previously published data on Permian intrusive rocks from the Kangguer–Huangshan shear zone are included to make a comprehensive analysis.

#### REGIONAL GEOLOGICAL BACKGROUND

The Tianshan Range, extending E-W from the Xinjiang Region (NW China) to Kyrgyzstan, Tajikistan and Uzbekistan for about 2500 km, is a young mountain belt due to the intra-continental shortening induced by the Tertiary Indo-Asia collision (Tapponnier and Molnar, 1979; Avouac and others, 1993; Shu and others, 2003). It is separated from the Tarim Basin in the south and the Junggar Basin in the north by two Cenozoic major fold-and-thrust belts (fig. 1B). The precursor of the present Tianshan is a Paleozoic accretionary/collisional belt that resulted from multiphase accretion and amalgamation of various micro-continents and magmatic arcs between the Kazakh, Junggar and Tarim continents (Coleman, 1989; Allen and others, 1993; Shi and others, 1994; Gao and others, 1998; Shu and others, 2000, 2004; Xiao and others, 2004; Kröner and others, 2007; Charvet and others, 2007, 2011; Wang and others, 2008a; Han and others, 2011).

Generally, the Chinese segment of the Tianshan Range, referred to as East Tianshan, is further divided into eastern and western parts along the Urumqi–Korla meridian (fig. 1B). Our study focuses mainly on the eastern Chinese Tianshan located to the south of Tu-Ha Basin (figs. 1 and 2). Tectonically, the Paleozoic Tianshan is divided into three subunits, namely South Tianshan, Central Tianshan and North Tianshan (Xiao and others, 1992). The South Tianshan is composed of ophiolitic mélanges and allochthonous lower Paleozoic sedimentary rocks that are deformed and locally metamorphosed (Wang and others, 1994, 2008a, 2011; Laurent-Charvet and others, 2002). The Central Tianshan unit comprises a Precambrian crystalline basement and overlying early Paleozoic arc-type volcanic and volcanoclastic rocks associated with subduction-related granitoids; both the basement and the magmatic arc-sequence are intensely deformed and overlain by unconformable Carboniferous marine clastic sediments (Ma and others, 1997; Shu and others, 2000). The North Tianshan consists mainly of Late Devonian to Carboniferous calc-alkaline volcanic and volcanoclastic rocks and associated intrusions developed upon an unknown basement (Charvet and

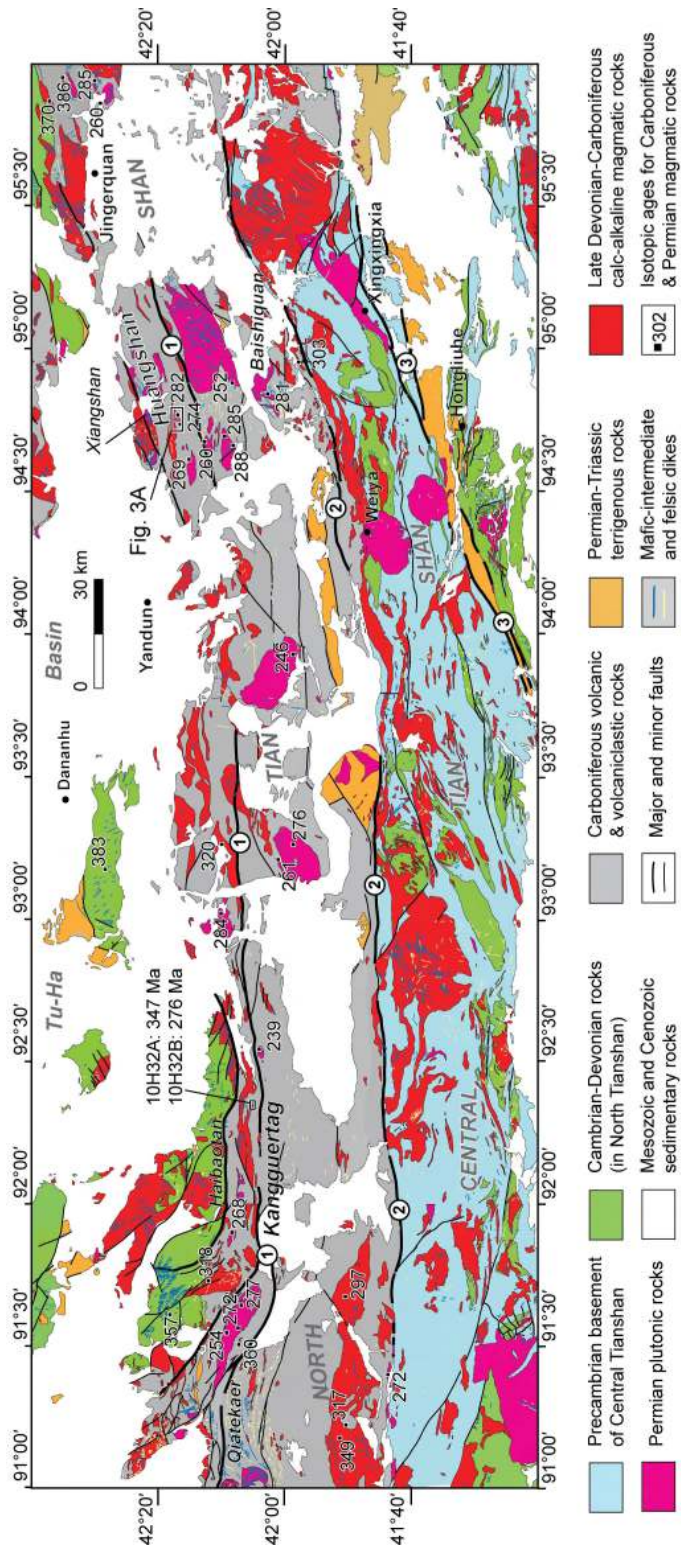


Fig. 2. Simplified geological map of the eastern Chinese North Tianshan compiled from geological maps at scale 1: 200 000. Numbers 1 to 3 stand for the Kangguer–Huangshan Shear Zone, Main Tianshan Shear Zone, and the Xingxingxia Fault, respectively. Location of map is shown in figure 1B.

others, 2007) (fig. 2). Permian rocks that occur sporadically in the three units are similar and include bimodal volcanic rocks in the lower part and red beds in the upper part (Li and others, 2006b; Shu and others, 2011).

The three units are separated from each other along two major faults; the Main Tianshan Shear Zone (MTSZ; Shu and others, 1999; Laurent-Charvet and others, 2002) and the Xingxingxia Fault (XXF; Charvet and others, 2007) (figs. 1B and 2). These faults reactivated older suture zones that are recognized as ophiolitic mélanges and record the pre-Permian accretion of the Central and South Tianshan units with the Tarim (Ma and others, 1997; Guo and others, 2002; Shu and others, 2004; Charvet and others, 2007, 2011). The formation of Late Devonian to late Carboniferous arc-related magmatic rocks in the North Tianshan is related to a southward subduction of the paleo-Junggar Ocean (Ma and others, 1997; Shu and others, 2000; Charvet and others, 2007, 2011) or, alternatively, is linked to the northward subduction of an oceanic basin located in the south of the North Tianshan (Allen and others, 1993; Li and others, 2002, 2006a).

Tectonic reactivation occurred in Permian to Triassic times along the boundaries of older units. The MTSZ and XXF and their westward continuations (Nalati Fault and North Tianshan Fault, fig. 1B) are generally dextral shear zones with local sinistral components (Shu and others, 1999; Laurent-Charvet and others, 2002, 2003; Wang and others, 2006a, 2008a, 2008c, 2010). Structural and paleomagnetic studies reveal that dextral strike-slip motion resulted from post-collisional relative rotation between continental blocks and accommodated eastward extrusion of the welded Central Tianshan and Yili-Junggar assemblage along the main shear zones (Wang and others, 2007, 2008c; Choulet and others, 2011).

#### KANGGUER–HUANGSHAN SHEAR ZONE

Within the North Tianshan unit a mega-shear zone, 5 to 25 km wide and ~600 km long, occurs along Kangguertag to the west and the Huangshan area to the east (fig. 2). The Kangguer–Huangshan Shear Zone is mainly occupied by Carboniferous sedimentary and volcanic rocks, including conglomerate, sandstone, graywacke, siltstone, bioclastic limestone, basaltic and/or andesitic tuff (XJBGMR, 1993). Devonian rocks only occur to the north of the shear zone and consist of basalt and andesite with minor rhyolite, dacite, volcanic breccia, tuff and clastic rocks. Lower Permian volcanic rocks recognized locally in the Kangguertag area unconformably overlie the Carboniferous sequence and are in turn overlain by middle and upper Permian colored arkose, interlayered with conglomerate (XJBGMR, 1993).

The Kangguer–Huangshan Shear Zone is characterized by intensive deformation and very low-grade metamorphism. Several publications have presented detailed structural analyses of this shear zone (Shu and others, 1999; Xu and others, 2003; Wang and others, 2008c; Branquet and others, 2012). Carboniferous rocks are affected by a mylonitic foliation and cleavage that are generally sub-vertical and oriented in a nearly E-W direction with NEE-SWW and SEE-NWW varieties in the Huangshan and Kangguertag areas, respectively (fig. 2). Chlorite schist and mica schist occur locally in the axial part of the Huangshan segment of the shear zone. Predominantly sub-horizontal stretching and mineral lineation are well developed on foliation surfaces in connection with transcurrent deformation, and are steeper locally.

The foliation on the northern and southern sides of the shear zone becomes shallower and dips to the south and north, respectively, to form a positive flower structure (Xu and others, 2003; Wang and others, 2008c). According to our observations, the foliation also varies along strike in the axial part of the shear zone. The foliation is curved and gradually changes in direction and dip as well, where it meets a pluton or a fold with vertical axis (figs. 2 and 3); in these locations the lineation

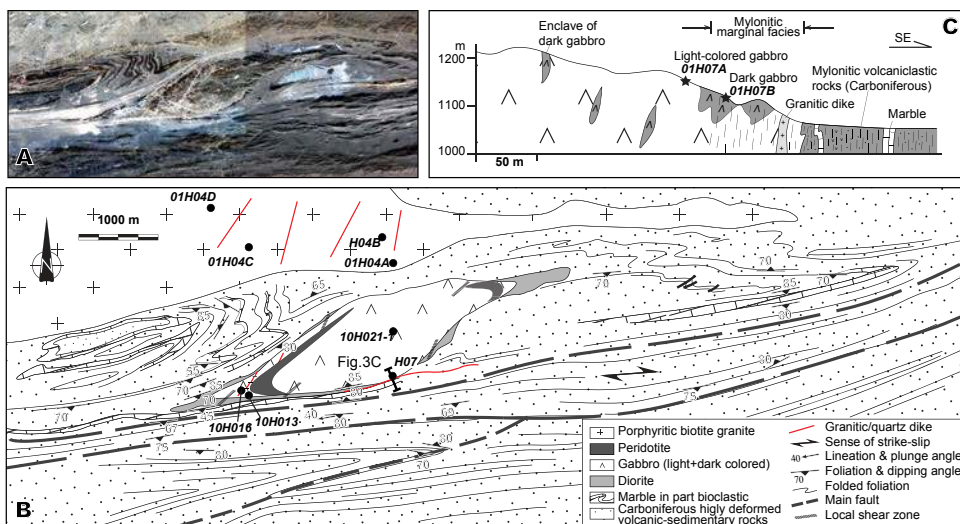


Fig. 3. (A) Satellite image (Google Earth) and (B) structural map of East Huangshan demonstrating the Permian sigmoidal intrusive complex, shear zone and Carboniferous granitic plutons; see figure 2 for map location. (C) Cross-section of East Huangshan intrusive complex showing sampling sites.

becomes steeper. These structures correspond to strain localization that is commonly recognized in shear zones.

Bedding can be recognized according to lithological transition; it is generally cut by, or transposed into, secondary cleavage or completely erased by mylonitic foliation. Bedding and early foliation are often tightly folded with sub-vertical or steeply dipping axes. Principal asymmetric folds as well as macro- and micro-kinematic indicators suggest a dextral sense of shear (Wang and others, 2008c; Branquet and others, 2012); whereas minor north-verging (Shu and others, 1999; Laurent-Charvet and others, 2002) or south-verging thrusts (Xu and others, 2003; Wang and others, 2008c), and local normal faulting can also be observed.

#### PRE- AND SYNKINEMATIC INTRUSIONS IN THE KANGGUER–HUANGSHAN SHEAR ZONE AND SAMPLING

Numerous late Paleozoic intrusions crop out in the eastern Chinese North Tianshan. Available geological maps show that Carboniferous intrusions mainly occur to the south of the Main Tianshan Shear Zone and to the north of Kangguer–Huangshan Shear Zone, whilst Permian intrusions of various sizes concentrate within and around the Kangguer–Huangshan Shear Zone, and also between the Main Tianshan Shear Zone and the Xingxing Fault (fig. 2). Abundant ore deposits are associated with the Permian intrusive rocks (Zhou and others, 2004; Han and others, 2006; Mao and others, 2008).

The Carboniferous intrusions consist of fine-grained biotite and/or hornblende granite, granodiorite, coarse-grained K-feldspar granite, biotite-bearing K-feldspar granite, and monzogranite (XJBGMR, 1993). They show homogeneous or porphyritic textures and massive structures, and are only weakly or not deformed. Sharp contacts between these intrusions and the strongly deformed Carboniferous volcano-sedimentary rocks can be observed. Most Carboniferous intrusions are cross-cut by faults displaying offsets of several meters to several kilometers (fig. 2). Along these narrow fault zones, no foliation/lineation and only slickensides and/or fractures can be

TABLE 1  
*Brief sample description and summary of geochronological results*

Sample	Section	Coordinate	Rock	Description	Age (Ma; this study)	Ages of inherited old zircons
01H04A	North of Huangshan	N42°17.217' E94°45.710'	Biotite granite	Porphyritic texture, undeformed	337.5 ± 3.8	376 Ma
01H07A	Southern margin of the East Huangshan intrusion	N42°16.334' E94°45.035'	Light-colored gabbro	Marginal facies, highly sheared	268.2 ± 2.1	
01H07B	Southern margin of the East Huangshan intrusion	N42°16.334' E94°45.035'	Melagabbro	Enclave/roof pendant in light-colored gabbro, sheared	274.5 ± 3.6	351, 362 Ma, 1.6 Ga
10H13	Westernmost of the East Huangshan intrusion	N42°16.268' E94°43.697'	Pyroxene diorite	Fine-grained, massive and undeformed	271.2 ± 3.8	455, 474 Ma
10H16	Westernmost of the East Huangshan intrusion	N42°16.271' E94°43.547'	Granitic dike	Undeformed, cut and offset by right lateral small fault	289.8 ± 1.3	
10H21-1	NE side of the East Huangshan intrusion	N42°16.738' E94°45.066'	Light-colored gabbro	Undeformed, but with magmatic layering	267.0 ± 2.1	
10H32A	East of Kangguertag	N42°05.669' E92°19.609'	K-feldspar granite	Fine-grained, massive, undeformed	346.9 ± 2.3	
10H32B	East of Kangguertag	N42°05.669' E92°19.609'	Gabbroic dike	Intruding K-granite 10H32A	273.5 ± 3.5	341, 390, 454 Ma; 1.3, 1.9, 2.2Ga

observed, indicating post-magmatic low-temperature brittle deformation. Five Carboniferous granitic rocks from East Huangshan and east of Kangguertag (samples 01H04A, B, C, D and 10H32A) were collected for zircon U-Pb dating and geochemical analyses; see table 1 and figures 2 and 3 for details of sampling locations, descriptions and summary of analytical results.

The Permian intrusions include mafic-ultramafic, intermediate and felsic plutons, some displaying several intrusion phases to form a composite intrusive complex. Specifically the East Huangshan and the western Huangshan mafic-ultramafic plutons are composed of peridotite and pyroxenite in the inner part, and gabbro and diorite in the external part (Branquet and others, 2012); in the Kangguertag–Juoluotag area, the Juoluotag pluton comprises diorite-granodiorite at its margins and granite-adamellite in the center (Wang and others, 2008c). The Permian intrusions or intrusive complexes outline particular shapes such as tongue-like (Juoluotag pluton), sigmoid (Huangshan intrusions; fig. 3A), tadpole-shape, hourglass- and flame-like small-scale intrusions (fig. 2). The tails of these spectacular bodies are generally parallel to the main foliation of strongly sheared country rocks, indicating synkinematic mega-fabrics consistent with dextral kinematics. Contact metamorphism is common in the country rocks in which aluminous mudstone and siltstone have recrystallized into andalusite and/or pyrophyllite-bearing black schist.

The margins of Permian mafic-ultramafic intrusions are strongly foliated showing a sub-vertical mylonitic foliation/cleavage associated with shear bands or S-C fabrics, which indicate a dextral sense of shearing (figs. 4A, 4B, 4C and 4E). In mafic intrusions, the deformation weakens inward and the shallow-dipping original compositional layering can be recognized (fig. 4D). However, localized shear bands also occur within the ultramafic and mafic intrusions. Various tectonic features can be distinguished such as ductile thrusts, low-angle normal shears and steep right-lateral shear zones (Branquet and others, 2012). Similar features can be observed in the Kangguertag (Juoluotag) tongue-shaped granitic complex (fig. 5A), in which quartz ribbons and biotite aggregates show shape-preferred orientation in external facies (fig. 5B). The orientation of crystals in the granite is parallel to the cleavage of the country rocks (black schist) and turns around along the granite border. The internal facies is characterized by a porphyritic texture with no preferred orientation of crystals. All these high-temperature ductile fabrics are diagnostic of syn- or late-magmatic crystallization of the intrusive rocks in a dynamic setting.

Mafic and felsic dikes and some intermediate dikes often cut through the Carboniferous and Permian intrusions (fig. 5C) as well as their country rocks, and show a principal orientation of SE-NW, and occasionally N-S and NNE-SSW (fig. 2). Quartz and/or pegmatite veins are also very common with the same orientation. Four mafic rocks (samples 10H07A, 07B, 10H13, 10H21-1) and one granite dike (sample 10H16) were collected from the East Huangshan area (fig. 3; table 1). In addition, one sample (10H32B) was collected from a melagabbro dike intruding Carboniferous granite (10H32A) in the Kangguertag area (fig. 2).

#### ANALYTICAL METHODS

Zircons were extracted from crushed material of eight samples (table 1) by (1) sieving to keep fractions of 140 to 250  $\mu\text{m}$ , (2) heavy-liquid and magnetic separation, and (3) handpicking under a binocular microscope. Zircons were then mounted in epoxy resin and polished. Cathodoluminescence (CL) images of zircons were undertaken at the State Key Laboratory of Continental Dynamics (Northwest University, Xi'an) with a Mono CL3+ machine connected with a Quanta 400 FEG scanning electron microscope (SEM). U-Pb isotopic analyses were conducted on an Agilent 7500s ICP-MS coupled with a New Wave 213  $\mu\text{m}$  laser ablation system at the State Key Laboratory for Mineral Deposits Research (Nanjing University). In order to trace

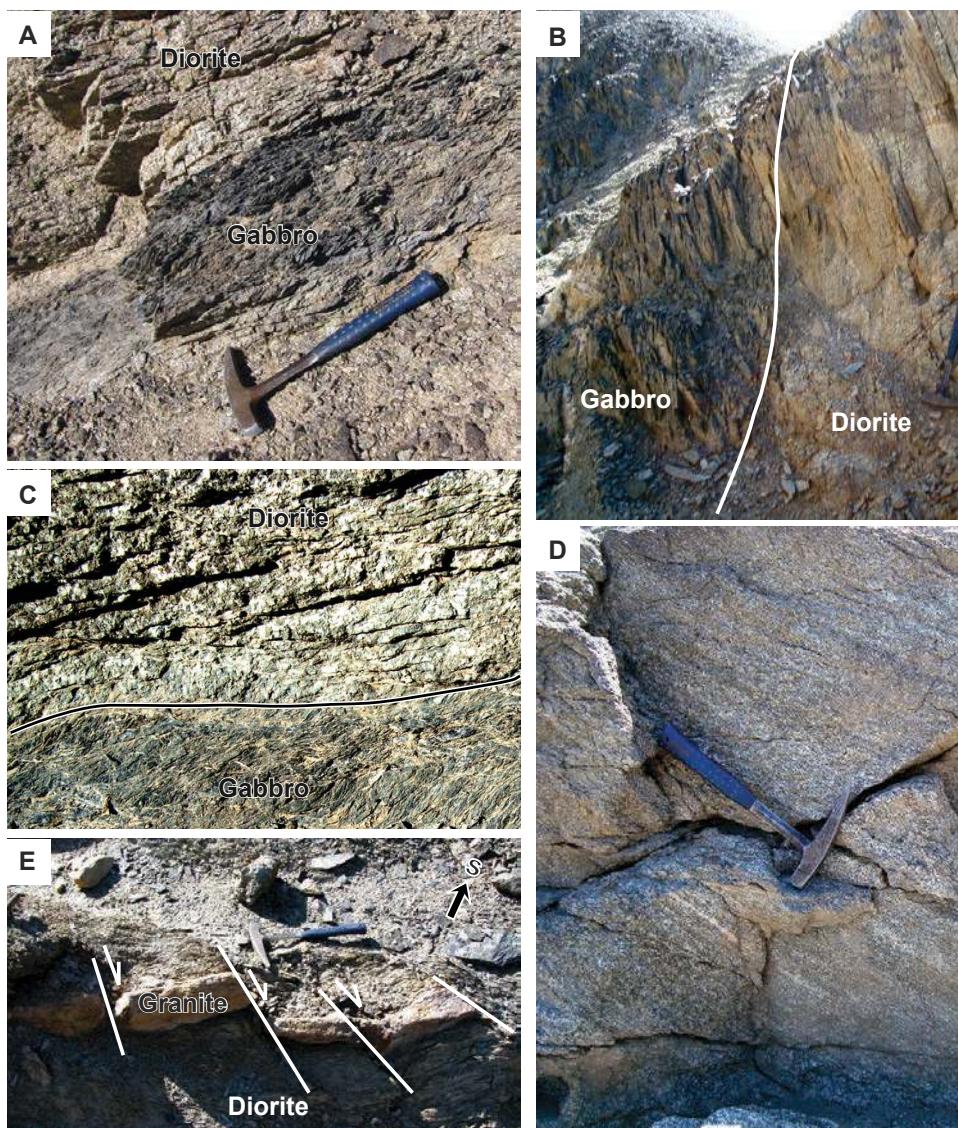


Fig. 4. Field photographs of the East Huangshan mafic complex. (A) Melagabbro enclave within light-colored gabbro; (B) intrusive contact between light-colored and dark gabbros; (C) mylonitic shear bands in melagabbro intruded by diorite; (D) compositional layering in light-colored gabbro; (E) granite dike surrounded by strongly sheared diorite, both are cut and offset by right lateral strike-slip faults.

instrument stability and to control analytical uncertainty, four analyses of internal standard zircon GJ ( $608 \pm 1.5$  Ma; Jackson and others, 2004) and one analysis of external standard zircon Mud Tank ( $732 \pm 5$  Ma; Black and others, 2003) were done for each ten analyses of unknown samples. Laser beam width varied from 30 to 50  $\mu\text{m}$  according to the size of analyzed zircon grains and target domains. Thereafter, U–Pb isotopic data were treated using the on-line software package GLITTER (ver. 4.4) (<http://www.mq.edu.au/GEMOC>). Correction for common lead was carried out using the Microsoft Excel embedded program ComPbCorr#3 15G by Andersen

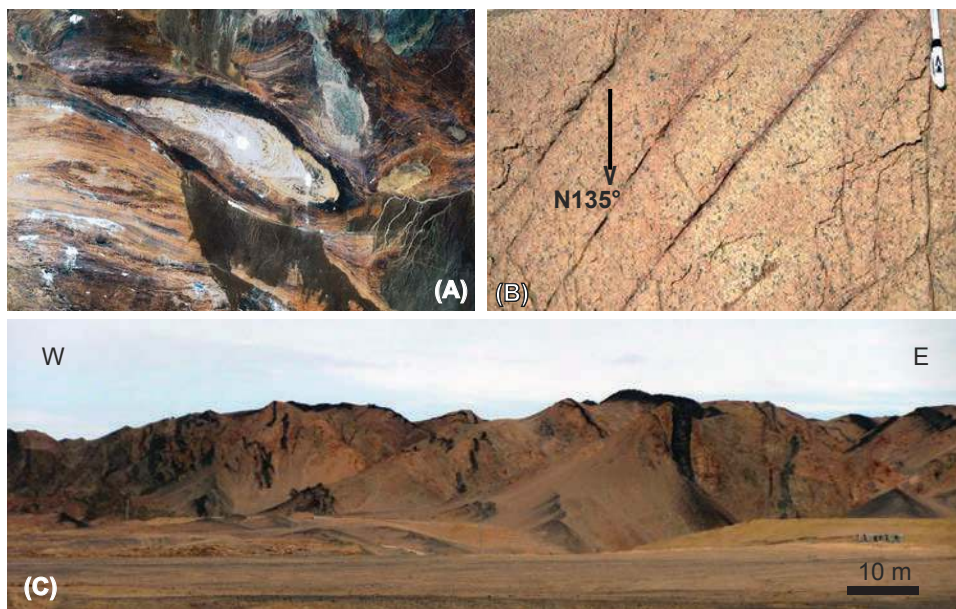


Fig. 5. (A) Satellite image (Google Earth) of the tongue-shaped granite pluton and shear zone in the Kanguertag area; (B) K-feldspar granite from SE side of the tongue-shaped pluton showing shape-preferred orientation (N135°) of biotite and quartz; (C) field view of the K-feldspar granite of Kanguertag and intruding mafic dikes with an overall SE-NW orientation.

(2002). Finally, the program ISOPLOT 3.1 (Ludwig, 2001) was applied for age calculation and plotting of analyses. We use the  $^{206}\text{Pb}/^{238}\text{U}$  apparent ages and errors to calculate average mean ages because the relatively small amount of  $^{207}\text{Pb}$  in Phanerozoic zircons may lead to low count rates and high analytical uncertainties (Compston and others, 1992). Uncertainties for individual analyses are quoted at  $1\sigma$  and for weighted mean ages at  $2\sigma$  (with 95% confidence level).

The powders of ten samples were analyzed for whole-rock chemical compositions. Major elements were determined using X-ray fluorescence (XRF) at the Modern Analysis Center of Nanjing University; the analytical procedures are similar to those described by Couture and others (1993). The analytical errors were 0.5 to 3 percent. Determination of Rare Earths (REE) and other trace elements were conducted on a HR-ICP-MS (Finnigan Element II) installed at the State Key Laboratory for Mineral Deposits Research of Nanjing University. The analytical technique was described by Gao and others (2003). Analytical errors are quoted at 0.7 to 5 percent for REE and trace elements.

## RESULTS

### *Zircon U-Pb Datings*

One porphyritic biotite granite (sample 01H04A) from the north of the East Huangshan mine has been dated by U-Pb zircon method. Zircons of this sample are euhedral, showing short prismatic to isometric or rhombic shapes (fig. 6A). Concentric oscillatory zoning is present in CL images of all dated zircons. Fourteen zircons were analyzed of which three analyses (No. 2, 6, 14) plot away from the Concordia (fig. 6B inset) probably due to partial Pb loss; two other analyses (No. 8, 9) yield consistent apparent  $^{206}\text{Pb}/^{238}\text{U}$  ages of  $378 \pm 8$  Ma and  $371 \pm 14$  Ma, respectively (table 2), and

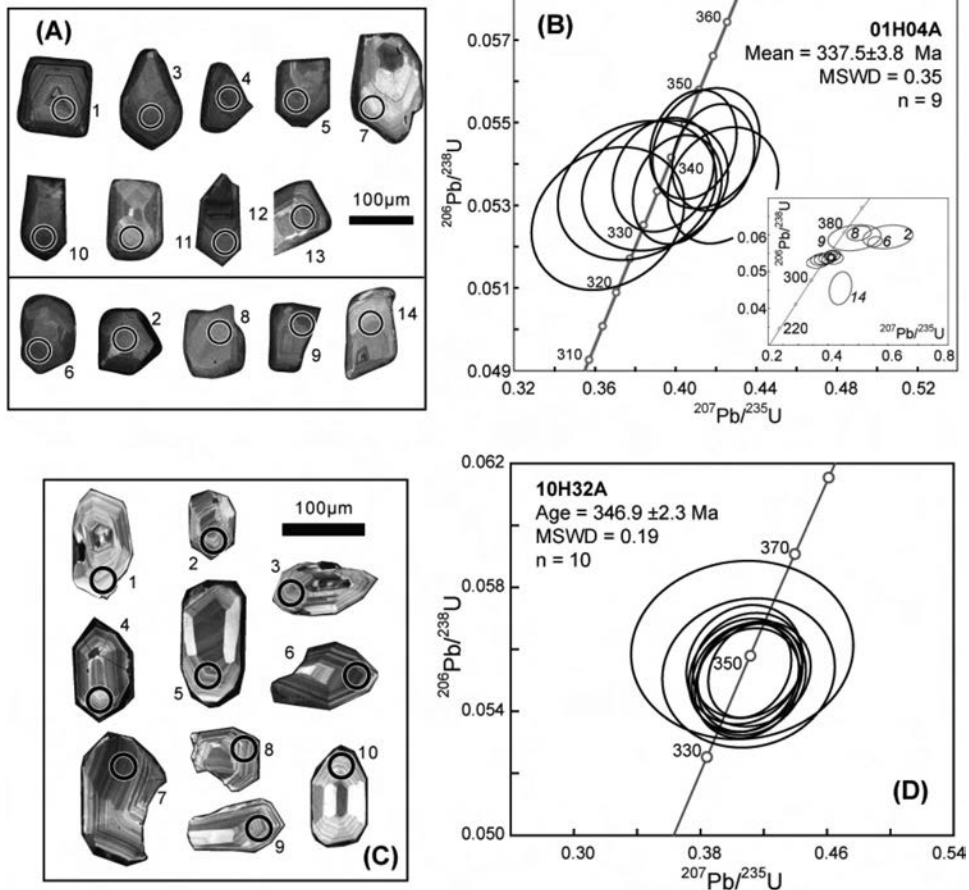


Fig. 6. Cathodoluminescence photographs and Concordia diagrams of LA-ICP-MS data of zircons from Carboniferous granites in the eastern Chinese North Tianshan.

thus could be xenocrysts and probably represent an earlier magmatic event. The other nine analyses plot on Concordia and yield consistent  $^{206}\text{Pb}/^{238}\text{U}$  ages from 331 Ma to 342 Ma (table 2), and a mean age of  $337.5 \pm 3.8$  Ma (MSWD = 0.35) (fig. 6B). This early Carboniferous age may be considered as the emplacement age of the porphyritic biotite granite.

Zircons selected from fine-grained K-feldspar granite (sample 10H32A) in the eastern Kangguertag area are characterized by euhedral, prismatic crystals with length/width ratios of 1.5 to 2; dense concentric oscillatory zoning as shown in CL images is in agreement with zircons from felsic rocks (fig. 6C). Inherited cores are suspected in some zircons (grains 1, 3) but are too small to be dated. Ten analyses plot on the Concordia and yielded consistent apparent  $^{206}\text{Pb}/^{238}\text{U}$  ages ranging from 345 Ma to 351 Ma, and a well defined concordant age at  $346.9 \pm 2.3$  (MSWD = 0.19; fig. 6D) constrains the early Carboniferous intrusion of this K-feldspar granite.

Six Permian intrusive rocks were dated. From the southeastern side of the East Huangshan mafic-ultramafic intrusive complex, a light-colored gabbro of the marginal facies (sample 01H07A) contains zircons with euhedral prismatic, isometric or irregular shapes. The CL images of these zircons are characterized by dark and widely spaced

TABLE 2

*LA-ICPMS analytical results of zircons from Carboniferous and Permian intrusive rocks of the eastern Chinese North Tianshan*

Analysis	$\frac{^{207}\text{Pb}}{^{206}\text{Pb}}$		Corrected ratios		$\frac{^{207}\text{Pb}}{^{235}\text{U}}$		$\frac{^{206}\text{Pb}}{^{238}\text{U}}$		Corrected ages (Ma)		$\frac{^{206}\text{Pb}}{^{238}\text{U}}$		Error correlation
	1 $\sigma$		1 $\sigma$		1 $\sigma$		1 $\sigma$		1 $\sigma$		1 $\sigma$		
Sample 01H04A, undeformed porphyritic biotite granite													
01H04A-01	0.05607	0.00182	0.41870	0.01350	0.05416	0.00085	455	74	355	10	340	5	0.23
01H04A-02	0.07315	0.00709	0.59933	0.05511	0.05943	0.00210	1018	204	477	35	372	13	0.05
01H04A-03	0.05446	0.00200	0.40081	0.01455	0.05338	0.00087	390	84	342	11	335	5	0.2
01H04A-04	0.06942	0.00203	0.55636	0.01613	0.05813	0.00091	911	62	449	11	364	6	0.25
01H04A-05	0.05316	0.00227	0.39385	0.01657	0.05374	0.00091	336	99	337	12	337	6	0.16
01H04A-06	0.05443	0.00191	0.40875	0.01419	0.05447	0.00087	389	81	348	10	342	5	0.21
01H04A-07	0.05177	0.00360	0.38082	0.02593	0.05336	0.00111	275	160	328	19	335	7	0.08
01H04A-08	0.06042	0.00334	0.50329	0.02685	0.06042	0.00130	619	123	414	18	378	8	0.11
01H04A-09	0.05975	0.00744	0.48768	0.05831	0.05920	0.00232	595	281	403	40	371	14	0.03
01H04A-10	0.05537	0.00239	0.41512	0.01757	0.05438	0.00096	427	99	353	13	341	6	0.16
01H04A-11	0.05044	0.00352	0.36636	0.02499	0.05268	0.00114	215	160	317	19	331	7	0.09
01H04A-12	0.05743	0.00250	0.42347	0.01812	0.05348	0.00093	508	98	359	13	336	6	0.16
01H04A-13	0.05287	0.00330	0.38979	0.02390	0.05348	0.00104	323	145	334	17	336	6	0.1
01H04A-14	0.07034	0.00599	0.44130	0.02461	0.04550	0.00293	938	181	371	17	287	18	0.1
Sample 10H32A, undeformed fine-grained K-feldspar granite													
10h32a-01	0.05266	0.00618	0.40638	0.04636	0.05598	0.00190	314	265	346	33	351	12	0.05
10h32a-02	0.05329	0.00323	0.40786	0.02422	0.05551	0.00127	341	141	347	17	348	8	0.14
10h32a-03	0.05412	0.00295	0.40968	0.02196	0.05491	0.00117	376	126	349	16	345	7	0.16
10h32a-04	0.05438	0.00313	0.41388	0.02362	0.05521	0.00112	387	133	352	17	346	7	0.15
10h32a-05	0.05361	0.00303	0.41006	0.02296	0.05548	0.00112	355	131	349	17	348	7	0.15
10h32a-06	0.05400	0.00283	0.41010	0.02121	0.05509	0.00115	371	121	349	15	346	7	0.17
10h32a-07	0.05374	0.00317	0.40860	0.02368	0.05516	0.00121	360	137	348	17	346	7	0.14
10h32a-08	0.05410	0.00319	0.41057	0.02384	0.05505	0.00120	375	136	349	17	345	7	0.15
10h32a-09	0.05389	0.00486	0.41040	0.03599	0.05524	0.00159	366	207	349	26	347	10	0.08
10h32a-10	0.05392	0.00226	0.41118	0.01733	0.05531	0.00100	368	97	350	12	347	6	0.23
Sample 01H07A, highly sheared light-colored gabbro intruding dark gabbro													
01H07A-01	0.05167	0.00100	0.30256	0.00606	0.04247	0.00056	271	45	268	5	268	3	0.38
01H07A-02	0.05074	0.00135	0.29606	0.00786	0.04232	0.00060	229	63	263	6	267	4	0.26
01H07A-03	0.05207	0.00100	0.30728	0.00609	0.04280	0.00057	288	45	272	5	270	4	0.38
01H07A-04	0.05275	0.00101	0.30637	0.00607	0.04213	0.00056	318	45	271	5	266	3	0.38
01H07A-05	0.05227	0.00104	0.30976	0.00636	0.04298	0.00058	297	46	274	5	271	4	0.37
01H07A-06	0.05171	0.00120	0.30864	0.00725	0.04329	0.00060	273	54	273	6	273	4	0.32

TABLE 2  
(continued)

Analysis	$\frac{^{207}\text{Pb}}{^{206}\text{Pb}}$		Corrected ratios		$\frac{^{207}\text{Pb}}{^{206}\text{Pb}}$		Corrected ages (Ma)		Error correlation			
	$1\sigma$		$1\sigma$		$1\sigma$		$1\sigma$					
Sample 01H07A, highly sheared light-colored gabbro intruding dark gabbro												
01H07A-07	0.05228	0.00089	0.30403	0.00544	0.00055	298	40	270	4	266	3	0.43
01H07A-08	0.05203	0.00084	0.30590	0.00524	0.00055	287	38	271	4	269	3	0.45
01H07A-09	0.06094	0.00205	0.36131	0.01195	0.00068	637	74	313	9	271	4	0.2
01H07A-10	0.05159	0.00166	0.30125	0.00957	0.00065	267	76	267	7	267	4	0.21
01H07A-11	0.05255	0.00299	0.30632	0.01679	0.00089	309	133	271	13	267	6	0.09
01H07A-12	0.05141	0.00114	0.30056	0.00679	0.00058	259	52	267	5	268	4	0.33
01H07A-13	0.04922	0.00125	0.29719	0.00757	0.00062	158	61	264	6	276	4	0.28
01H07A-14	0.05895	0.00221	0.31310	0.00570	0.00126	565	84	277	4	244	8	0.1
Sample 01H07B, highly sheared melagabbro (roof pendant intruded by light-colored gabbro)												
01H07B-01	0.05092	0.00142	0.31106	0.00869	0.00066	237	66	275	7	279	4	0.27
01H07B-02	0.05330	0.00204	0.32274	0.01206	0.00075	342	89	284	9	277	5	0.17
01H07B-03	0.05339	0.00084	0.31791	0.00542	0.00057	345	36	280	4	273	4	0.48
01H07B-04	0.05414	0.00107	0.31827	0.00657	0.00059	377	45	281	5	269	4	0.4
01H07B-05	0.06051	0.00109	0.48239	0.00918	0.00079	622	40	400	6	362	5	0.43
01H07B-06	0.05850	0.00276	0.35475	0.01612	0.00087	549	106	308	12	277	5	0.13
01H07B-07	0.09761	0.00123	3.46071	0.05027	0.00337	1579	24	1518	11	1475	17	0.59
01H07B-08	0.08296	0.00806	0.34699	0.03263	0.00074	1268	197	302	25	193	5	0.39
01H07B-09	0.05372	0.00069	0.31780	0.00466	0.00056	359	30	280	4	271	3	0.58
01H07B-10	0.09319	0.00947	0.49272	0.04795	0.00113	1492	200	407	33	243	7	0.3
01H07B-11	0.05216	0.00068	0.31318	0.00467	0.00057	292	30	277	4	275	4	0.57
01H07B-12	0.05904	0.00148	0.45511	0.01146	0.00082	569	56	381	8	351	5	0.3
01H07B-13	0.05270	0.00089	0.31853	0.00574	0.00059	316	39	281	4	277	4	0.45
Sample 10H1, fine-grained undeformed diorite												
10H13-01	0.05286	0.00203	0.31126	0.01191	0.00079	323	89	275	9	270	5	0.23
10H13-02	0.05117	0.00169	0.30593	0.01027	0.00074	248	78	271	8	274	5	0.29
10H13-03	0.05622	0.00205	0.32497	0.01187	0.00076	461	83	286	9	265	5	0.25
10H13-04	0.05548	0.00128	0.31914	0.00784	0.00067	432	53	281	6	263	4	0.42
10H13-05	0.05618	0.00135	0.59048	0.01505	0.00123	459	55	471	10	474	7	0.4
10H13-06	0.05655	0.00195	0.57062	0.01977	0.00132	474	78	458	13	455	8	0.27
10H13-07	0.06295	0.00167	0.36560	0.01002	0.00070	707	58	316	7	266	4	0.36
10H13-08	0.05219	0.00114	0.31156	0.00736	0.00068	294	51	275	6	273	4	0.44
10H13-09	0.05138	0.00130	0.30911	0.00819	0.00071	258	60	273	6	275	4	0.38

TABLE 2  
(continued)

Analysis	Corrected ratios		Corrected ages (Ma)		Error correlation							
	$\frac{^{207}\text{Pb}}{^{235}\text{U}}$	$\frac{^{206}\text{Pb}}{^{238}\text{U}}$	$\frac{^{207}\text{Pb}}{^{235}\text{U}}$	$\frac{^{206}\text{Pb}}{^{238}\text{U}}$								
Sample 10H1, fine-grained undeformed diorite												
10H13-10	0.05163	0.00129	0.31145	0.00819	0.00071	269	59	275	6	276	4	0.39
10H13-11	0.05152	0.00176	0.31227	0.01078	0.00078	264	80	276	8	277	5	0.28
10H13-12	0.05386	0.00112	0.31381	0.00711	0.00066	365	48	277	5	267	4	0.46
10H13-13	0.05461	0.00171	0.31566	0.01006	0.00073	396	72	279	8	265	5	0.3
10H13-14	0.05177	0.00150	0.31708	0.00943	0.00074	275	68	280	7	280	5	0.33
Sample 10H16, fine-grained massive granitic dike												
10H16-01	0.05276	0.00109	0.33323	0.00761	0.00071	318	48	292	6	289	4	0.47
10H16-02	0.05204	0.00129	0.33430	0.00885	0.00074	287	58	293	7	294	5	0.4
10H16-03	0.05412	0.00237	0.33467	0.01453	0.00087	376	101	293	11	283	5	0.2
10H16-04	0.05257	0.00129	0.33318	0.00869	0.00073	310	57	292	7	290	4	0.4
10H16-05	0.05295	0.00098	0.33420	0.00701	0.00071	327	43	293	5	289	4	0.52
10H16-06	0.05142	0.00131	0.32660	0.00882	0.00073	260	60	287	7	290	4	0.39
10H16-07	0.05140	0.00192	0.32929	0.01242	0.00081	259	88	289	9	293	5	0.25
10H16-08	0.05327	0.00162	0.33355	0.01042	0.00077	340	70	292	8	286	5	0.32
10H16-09	0.05213	0.00126	0.33151	0.00851	0.00074	291	57	291	6	291	5	0.4
10H16-10	0.05384	0.00156	0.33576	0.01009	0.00074	364	67	294	8	285	5	0.34
10H16-11	0.05126	0.00117	0.33030	0.00810	0.00074	253	54	290	6	294	5	0.43
10H16-12	0.05231	0.00128	0.33138	0.00857	0.00074	299	57	291	7	290	5	0.4
Sample 10H21-1, undeformed gabbro with magmatic layering												
10h21-01	0.05102	0.00069	0.30162	0.00463	0.00057	242	32	268	4	271	4	0.56
10h21-02	0.05167	0.00091	0.30355	0.00570	0.00058	271	41	269	4	269	4	0.45
10h21-03	0.05195	0.00085	0.30113	0.00533	0.00057	283	38	267	4	266	4	0.48
10h21-04	0.07106	0.00245	0.30760	0.00601	0.00089	959	72	272	5	199	6	0.41
10h21-05	0.05194	0.00077	0.29830	0.00488	0.00055	283	35	265	4	263	3	0.51
10h21-06	0.05066	0.00074	0.29587	0.00480	0.00056	225	35	263	4	268	3	0.52
10h21-07	0.05128	0.00072	0.30030	0.00475	0.00056	253	33	267	4	268	3	0.54
10h21-08	0.05187	0.00071	0.30281	0.00468	0.00056	280	32	269	4	267	3	0.55
10h21-09	0.06885	0.00257	0.29633	0.00642	0.00095	894	79	264	5	198	6	0.37
10h21-10	0.05246	0.00091	0.30292	0.00561	0.00057	306	40	269	4	264	4	0.45
10h21-11	0.05174	0.00108	0.30168	0.00654	0.00060	274	49	268	5	267	4	0.38
10h21-12	0.05071	0.00099	0.29739	0.00610	0.00059	228	46	264	5	269	4	0.41

TABLE 2  
(continued)

Analysis	$\frac{^{207}\text{Pb}}{^{206}\text{Pb}}$		Corrected ratios		$\frac{^{206}\text{Pb}}{^{238}\text{U}}$		$\frac{^{207}\text{Pb}}{^{206}\text{Pb}}$		Corrected ages (Ma)		$\frac{^{206}\text{Pb}}{^{238}\text{U}}$		Error correlation	
	1 $\sigma$		1 $\sigma$		1 $\sigma$		1 $\sigma$		1 $\sigma$		1 $\sigma$			
Sample 10H21-1, undeformed gabbro with magmatic layering														
10h21-13	0.05210	0.00088	0.30234	0.00547	0.04210	0.00057	290	268	4	266	4	266	4	0.46
10h21-14	0.07216	0.00252	0.31684	0.00615	0.03184	0.00092	991	279	5	202	5	202	6	0.41
Sample 10H32B, gabbroic dike intruding K-granite 10H32A														
10h32b-01	0.05165	0.00173	0.32859	0.01120	0.04614	0.00084	270	288	9	291	9	291	5	0.3
10h32b-02	0.05535	0.00207	0.47746	0.01799	0.06257	0.00117	426	396	12	391	12	391	7	0.26
10h32b-03	0.06095	0.00199	0.36235	0.01208	0.04312	0.00076	637	314	9	272	9	272	5	0.3
10h32b-04	0.05540	0.00247	0.47825	0.02143	0.06262	0.00117	428	397	15	392	15	392	7	0.22
10h32b-05	0.05834	0.00138	0.58177	0.01474	0.07234	0.00120	543	466	9	450	9	450	7	0.43
10h32b-06	0.11905	0.00166	5.63976	0.09878	0.34360	0.00543	1942	1922	15	1904	15	1904	26	0.65
10h32b-07	0.05461	0.00244	0.33021	0.01458	0.04386	0.00090	396	290	11	277	11	277	6	0.21
10h32b-08	0.06118	0.00204	0.58132	0.01958	0.06893	0.00128	646	465	13	430	13	430	8	0.29
10h32b-09	0.08571	0.00115	2.85276	0.04920	0.24143	0.00377	1332	1370	13	1394	13	1394	20	0.67
10h32b-10	0.05867	0.00139	0.59403	0.01509	0.07345	0.00123	555	473	10	457	10	457	7	0.43
10h32b-11	0.05160	0.00148	0.30904	0.00927	0.04344	0.00073	268	273	7	274	7	274	5	0.36
10h32b-12	0.05308	0.00156	0.45224	0.01387	0.06180	0.00105	332	379	10	387	10	387	6	0.35
10h32b-A1	0.05612	0.00150	0.42553	0.01135	0.05500	0.00077	457	360	8	345	8	345	5	0.26
10h32b-A2	0.05077	0.00192	0.38701	0.01442	0.05529	0.00085	230	332	11	347	11	347	5	0.17
10h32b-A3	0.60787	0.03712	13.10681	0.59636	0.15640	0.00734	4527	2687	43	937	43	937	41	0.13
10h32b-A4	0.05498	0.00275	0.41216	0.02002	0.05438	0.00101	411	350	14	341	14	341	6	0.11
10h32b-A5	0.05603	0.00144	0.43082	0.01113	0.05577	0.00077	454	364	8	350	8	350	5	0.28
10h32b-A6	0.05114	0.00300	0.30138	0.01723	0.04274	0.00058	247	267	13	270	13	270	4	0.44
10h32b-A7	0.05092	0.00363	0.30355	0.02120	0.04324	0.00063	237	269	17	273	17	273	4	0.47
10h32b-A9	0.06213	0.00850	0.35107	0.04747	0.04098	0.00084	679	306	36	259	36	259	5	0.58
10h32b-A8	0.05938	0.00304	0.35657	0.01779	0.04356	0.00079	581	310	13	275	13	275	5	0.11
10h32b-B0	0.05313	0.00233	0.39654	0.01652	0.05413	0.00076	334	339	12	340	12	340	5	0.31
10h32b-B1	0.06075	0.00401	0.44188	0.02813	0.05276	0.00122	630	372	20	331	20	331	7	0.08
10h32b-B2	0.13756	0.02480	7.10108	1.22740	0.37445	0.02504	2197	2124	154	2050	154	2050	117	0.08

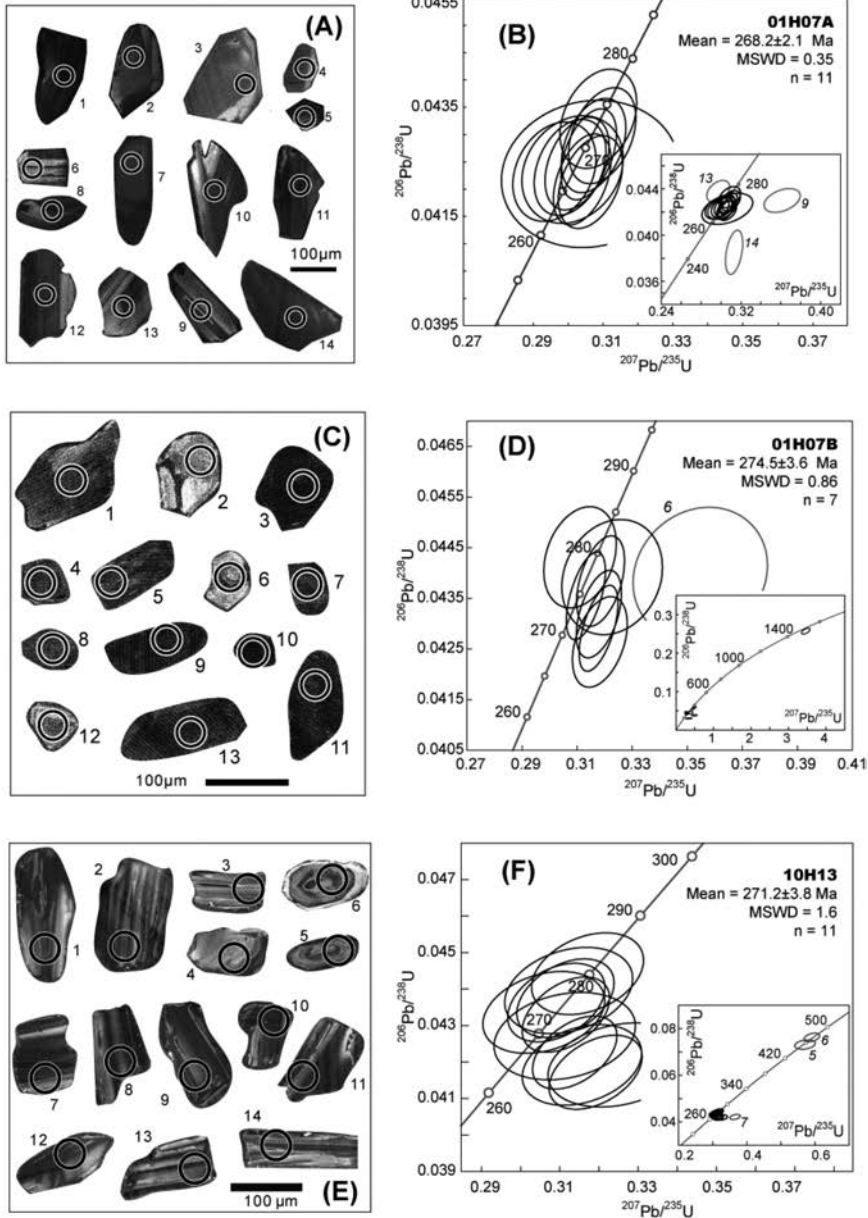


Fig. 7. Cathodoluminescence photographs and Concordia diagrams of LA-ICP-MS U-Pb data of zircons from gabbroic samples of the East Huangshan intrusive complex.

oscillatory zoning (fig. 7A), consistent with a magmatic origin of high-temperature zircon in mafic rocks (Corfu and others, 2003). Fourteen zircons were analyzed of which two analyses (No. 9 and 14) yielded discordant ages probably due to lead loss, and analysis No. 13 plots above the Concordia (fig. 7B). These three analyses are not considered in the mean age calculation. The other 11 zircons yielded consistent concordant apparent ages (table 2) and a well defined mean age at  $268.2 \pm 2.1$  Ma (fig.

7B) that may represent the middle Permian crystallization age of the light-colored gabbro.

The roof pendant melagabbro (sample 01H07B) is intruded by a light-colored gabbro (01H07A) and contains very few zircons with variable shapes and sizes ranging from 50 to 150  $\mu\text{m}$  (fig. 7C). Oscillatory zoning can hardly be recognized in CL images due to intense surface-controlled alteration (Vavra and others, 1996; fig. 7C) that is probably related to thermal or fluid-assisted overprint. However, striped oscillatory zoning can be observed in zircons No. 1 and 5, consistent with their gabbroic magmatic origin. Only thirteen zircons were datable; one zircon (grain No. 7) yielded a concordant apparent age of  $\sim 1500$  Ma (table 2), and two other zircons (No. 5 and 12) yielded nearly concordant ages of 351 to 362 Ma (apparent  $^{206}\text{Pb}/^{238}\text{U}$  ages table 2). These zircons probably are xenocrysts derived from old crust, captured during emplacement of the melagabbro. Three analyses (No. 6, 8 and 10) plot away from the Concordia; their old apparent  $^{207}\text{Pb}/^{206}\text{Pb}$  ages indicate that they are probably xenocrysts but were strongly overprinted during the magmatism. The remaining seven zircons yielded consistent apparent ages and a mean age of  $274.5 \pm 3.6$  Ma (MSWD = 0.86) (fig. 7D). This can be considered as the early Permian emplacement age of the melagabbro, and it is  $\sim 10$  Ma older than the intruding light-colored gabbro.

Fourteen zircons were dated from the pyroxene-diorite (sample 10H13) taken from the westernmost side of the East Huangshan intrusive complex. Except for two zircons (No. 5 and 6) showing typical prismatic shapes and concentric oscillatory zoning with light overgrowth rims, the other samples are lath-shaped, and characterized by striped oscillatory zoning (fig. 7E). Zoning-controlled alteration is commonly observed on the CL images of all analyzed zircons (Vavra and others, 1996). Zircons No. 5 and 6 yielded ages of 455 to 474 Ma, which are much older than the ages obtained from the other zircons, and therefore most likely indicate inheritance. One zircon (No. 7) yielded a discordant apparent age. The other eleven analyses plot on or close to Concordia, and their apparent ages were used to calculate a mean age of  $271.2 \pm 3.8$  Ma (fig. 7F) that constrains the early Permian emplacement of the pyroxene-diorite.

Sample 10H16 was collected from a granitic dike that crops out in the southwestern side of the East Huangshan intrusive complex; it is cut by right-lateral strike-slip faults (fig. 4). Twelve zircons were selected for U-Pb analysis; most zircons are euhedral, prismatic and show concentric oscillatory zoning, and others show rounded or short prismatic shapes and irregular oscillatory zoning in CL images (fig. 8A). All dated zircons yielded consistent isotopic ratios that define a concordant early Permian age of  $289.8 \pm 1.3$  Ma (MSWD = 0.73; fig. 8B).

Fourteen zircons were analyzed from a light-colored gabbro that shows magmatic layering (sample 10H21-1). These zircons are characterized by long prismatic shapes with high length/width ratios of 1.5 to 4 and typical widely striped oscillatory zoning, indicative of a mafic magmatic origin (fig. 8C). Except for three zircons (No. 4, 9 and 14; table 2) yielding discordant ages probably due to lead loss, the other eleven analyses plot on Concordia and provide a well-defined concordant age of  $267.0 \pm 2.1$  Ma (MSWD = 0.23; fig. 8D). This middle Permian age is consistent with the age of the aforementioned light-colored gabbro sample (01H07A).

About 30 zircons were extracted from the dark gabbroic dike (sample 10H32B) that intrudes the early Carboniferous K-feldspar granite (sample 10H32A). These zircons are generally small ( $\sim 100$   $\mu\text{m}$ ) with low length/width ratios ( $\sim 1$ -1.2), and therefore only 24 zircons could be dated. The results can be subdivided into several groups. (1) Grain No. A3 shows a light CL image without visible oscillatory zoning (fig. 8E), plots far away from Concordia (fig. 8F), and has an unusually old apparent  $^{207}\text{Pb}/^{206}\text{Pb}$  age ( $\sim 4.5$  Ga). It is possible that a titanite grain was dated. (2) Three

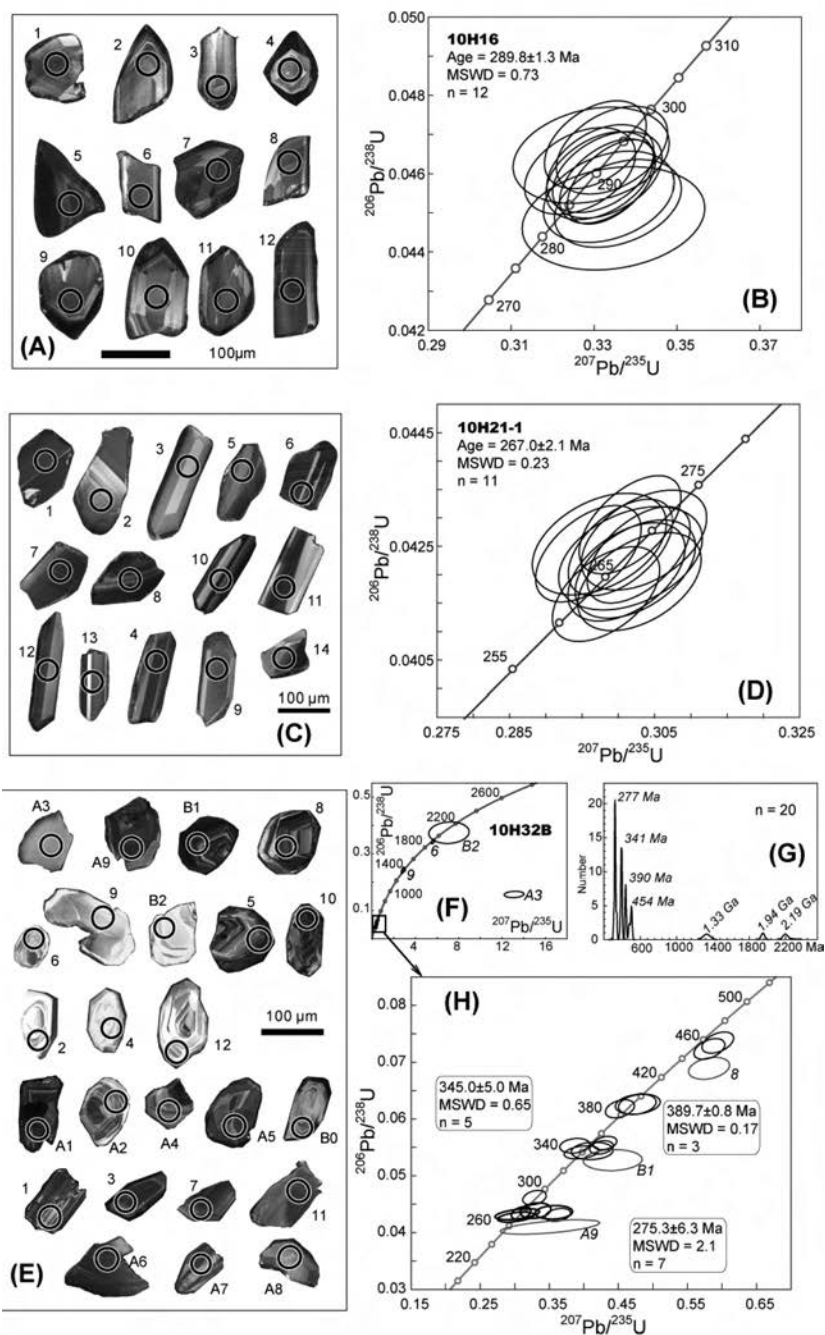


Fig. 8. Cathodoluminescence photographs and Concordia diagrams of LA-ICP-MS U-Pb data of zircons from Permian intrusive rocks in the eastern Chinese North Tianshan.

zircons (No. 6, 9 and B2) are characterized by bright CL images with obvious magmatic zoning (fig. 8E), and yielded old concordant ages of ~1940 Ma, ~1330 Ma and ~2190 Ma, respectively (table 2; figs. 8F and 8G). (3) Zircons No. 5, 8 and 10 have similar CL images and yielded nearly consistent apparent ages (~430-457 Ma) to form a peak at ~454 Ma on the probability density plot (fig. 8G). Analysis No. 8 plots away from Concordia (fig. 8H) probably due to thermal alteration of an old inherited zircon as shown on its CL image (fig. 8E). (4) One group composed of three zircons (No. 2, 4 and 12) is of felsic magmatic origin according to their similarly bright CL images showing concentric oscillatory zoning, and the analytical results plot on Concordia defining a mean age at  $389.7 \pm 0.8$  Ma (MSWD = 0.17) (fig. 8H). (5) Six zircons (No. A1, A2, A4, A5, B0 and B1) show variable CL images, but yielded nearly consistent and concordant apparent ages except for one grain (No. B1) that shows possible zoning-controlled alteration (fig. 8E); the ages of the other five zircons provide a mean age of  $345.0 \pm 5.0$  Ma (MSWD = 0.65) (fig. 8H). The zircons in groups 2–5 are inherited grains, entrained by the mafic magma, but the oldest ones may reflect the existence of underlying Precambrian continental crust. In addition, the occurrence of Carboniferous zircons signals the existence of underlying Carboniferous rocks, which is consistent with the occurrence of arc-related magmatic rocks at ~320 to 380 Ma in the North Tianshan (fig. 2) (Li and others, 2002, 2006a). (6) Finally, the analytical results for the remaining eight zircons plot close to Concordia, but one zircon (No. A9) is not considered because of its discordant apparent age and obviously different CL image from the other seven zircons. The CL images of these seven zircons show similar striped or poorly defined concentric oscillatory zoning, reflecting an origin from mafic magma. Their results define a mean age at  $275.3 \pm 6.3$  Ma (MSWD = 2.1) that may constrain the early Permian age of the gabbro intrusion.

#### *Whole-Rock Geochemistry*

Except for the granitic dike in the Huangshan area, all dated samples, including four mafic rocks of the East Huangshan intrusive complex, one porphyritic biotite granite and its three duplicate samples, one K-feldspar granite and cross-cutting gabbroic dike from the Kangguertag area were analyzed for whole-rock geochemical composition (see figs. 2 and 3 for sampling sites). The results are listed in table 3. All rocks have low loss on ignition values (LOI < 3.2 wt%), suggesting that they experienced little post-magmatic alteration. Except for the gabbroic dike, most rocks have high total alkali contents and plot along the calc-alkaline/subalkaline and alkaline division line (Wilson, 1989; fig. 9).

The Carboniferous granitic rocks are characterized by low  $\text{Al}_2\text{O}_3$  (<14 wt%) and CaO (1.1-2.1 wt%) contents, Mg# values (0.38-0.42) and A/CNK index (0.88-0.93). They show similarly LREE-enriched and HREE-flat patterns with moderate negative Eu anomalies (fig. 10A). These features are consistent with those of typical calc-alkaline magmatic rocks. Depletion in Nb, Ta, Sr and Eu can be recognized on the primitive mantle-normalized multi-element variation diagram (fig. 10B). The older K-feldspar granite from the Kangguertag area has lower HREE and total REE contents and more pronounced Nb and Ta depletion than the younger porphyritic biotite granites of the Huangshan area (fig. 10).

The Permian mafic rocks have high CaO (8.71-11.27 wt%) contents and Mg# values (0.56-0.71) (table 3). The dark gabbro shows a LREE-depleted REE pattern that is similar to N-MORB, but the contents of HREE decrease with increasing atomic number (fig. 11A). The other four mafic rocks consistently display flat REE patterns with slight enrichment in LREE, comparable to that of E-MORB, both in bulk REE content and distribution patterns. Positive Eu anomalies (1.64-1.82) are observed in the light-colored gabbro (10H07A, 10H21-1; table 3; fig. 11B) and may result from feldspar accumulation, consistent with the magmatic layering observed in the sample

TABLE 3

*Whole-rock geochemical data for magmatic rocks in the eastern Chinese North Tianshan*

Sample No.	01H04A	01H04B	01H04c	01H04D	10H07A	10H07B	10H13	10H21-1	10H32A	10H32B
	Undeformed porphyritic granite				Light colored gabbro	Mela-gabbro	Pyroxene diorite	Light colored gabbro	K- feldspar granite	Gabbro dike
SiO <sub>2</sub> (wt%)	69.7	71.5	71.2	70.2	50.1	47.0	52.7	50.1	75.1	48.8
TiO <sub>2</sub>	0.45	0.38	0.39	0.42	1.01	0.76	0.82	0.59	0.23	1.75
Al <sub>2</sub> O <sub>3</sub>	14.0	13.9	14.0	14.0	21.0	12.3	16.3	19.3	12.3	15.8
Fe <sub>2</sub> O <sub>3</sub>	2.84	2.27	2.56	2.77	5.1	11.3	7.24	6.35	1.43	11.0
MnO	0.10	0.07	0.09	0.10	0.07	0.16	0.12	0.10	0.06	0.17
MgO	0.92	0.71	0.70	0.75	4.89	12.6	7.46	7.07	0.47	6.44
CaO	2.11	1.48	1.09	1.12	10.5	11.3	8.71	11.1	0.87	9.63
Na <sub>2</sub> O	5.20	5.67	5.71	5.66	4.30	1.79	3.55	3.57	4.84	3.95
K <sub>2</sub> O	3.29	3.48	3.70	3.80	0.21	0.23	0.96	0.31	3.42	0.69
P <sub>2</sub> O <sub>5</sub>	0.07	0.05	0.05	0.06	0.06	0.01	0.08	0.03	0.01	0.25
LOI	1.58	0.75	1.10	1.13	3.18	2.23	2.60	1.93	0.63	1.68
Total	100.3	100.3	100.7	100.1	100.4	99.8	100.6	100.5	99.5	100.3
A/CNK <sup>1</sup>	0.88	0.88	0.91	0.91	0.79	0.52	0.72	0.73	0.93	0.64
Mg# <sup>2</sup>	0.42	0.41	0.38	0.37	0.68	0.71	0.69	0.71	0.42	0.56
Li(ppm)	12.3	9.40	10.4	9.20	12.7	12.8	18.7	9.01	9.07	
Sc	9.58	6.75	6.27	7.25	21.6	41.8	26.4	25.1	4.44	37.8
Ti	2524	2116	2048	2270	5286	4146	4560	3128	1355	9928
V	20.1	17.3	14.7	16.6	215	421	168	279	13.4	303
Cr	7.11	4.81	10.1	4.42	124	230	241	119	3.29	115
Mn	640	483	569	650	492	1091	794	642	501	1131
Co	2.04	1.59	1.32	1.46	17.1	39.7	23.0	23.4	1.53	30.4
Ni	3.34	1.86	4.20	1.34	13.5	39.7	17.9	14.1	1.39	41.2
Cu	2.08	3.31	1.38	1.29	12.5	23.5	10.7	18.3	3.27	67.5
Zn	58.3	29.5	38.9	39.3	29.2	43.2	45.5	28.3	34.0	52.7
Ga	19.1	16.0	18.0	19.2	16.3	11.2	16.6	14.2	13.5	18.9
Rb	28.7	31.5	36.8	40.6	3.93	2.65	19.6	4.16	45.2	8.23
Sr	126	141	122	125	488	258	338	394	89.9	372
Y	49.9	39.4	39.3	43.0	13.0	15.8	17.0	11.0	15.6	26.4
Zr	402	326	353	355	63.6	45.1	93.5	46.9	193	145
Nb	11.4	10.1	8.91	9.90	1.97	1.04	2.33	1.12	4.61	4.38
Mo	0.85	1.01	0.81	0.61	0.64	0.36	0.16	0.29	1.87	0.81
Cd	0.05	0.01	0.04	0.03	0.00	0.00	0.00	0.00	0.02	0.11
Sn	3.66	2.27	2.06	2.20	0.85	0.38	0.84	0.90	1.10	1.12
Cs	0.52	0.86	1.00	1.24	0.33	0.28	1.16	0.33	0.49	0.37
Ba	431	432	420	447	61.5	37.7	213	69.3	624	124
La	25.7	19.6	22.6	23.9	5.18	3.18	8.23	3.60	16.1	9.42
Ce	61.2	40.2	42.6	46.3	12.3	8.54	18.6	9.10	32.3	23.7
Pr	8.15	6.33	6.93	7.46	1.78	1.43	2.51	1.32	4.23	3.52
Nd	35.9	27.3	29.8	31.8	8.30	7.65	11.3	6.49	16.4	17.1
Sm	8.18	6.17	6.59	7.18	2.13	2.48	2.82	1.77	3.35	4.65
Eu	1.84	1.48	1.36	1.45	1.21	0.99	1.00	1.16	0.64	1.75
Gd	8.28	6.62	6.54	7.37	2.39	3.08	3.13	2.14	2.80	5.46
Tb	1.27	1.03	1.02	1.13	0.36	0.47	0.46	0.31	0.41	0.82
Dy	9.20	7.51	7.40	8.20	2.54	3.41	3.37	2.36	2.74	5.59
Ho	2.17	1.81	1.72	1.94	0.56	0.80	0.74	0.52	0.62	1.25
Er	6.49	5.30	5.03	5.78	1.54	2.12	2.13	1.42	1.81	3.54
Tm	0.97	0.82	0.77	0.87	0.21	0.30	0.29	0.19	0.27	0.50
Yb	6.59	5.60	5.24	5.90	1.31	1.71	1.93	1.23	1.84	3.01
Lu	1.01	0.82	0.80	0.85	0.20	0.26	0.28	0.18	0.30	0.47
Hf	10.2	8.46	8.90	9.21	1.58	1.37	2.57	1.34	5.00	3.87
Ta	0.97	0.88	0.78	0.85	0.23	0.10	0.22	0.11	0.36	0.39
W	0.87	0.37	0.53	0.55	0.79	0.18	0.33	0.18	0.37	0.21
Pb	5.69	4.04	4.42	4.82	2.49	1.11	4.19	1.46	11.9	2.72
Bi	0.07	0.05	0.03	0.04	0.02	0.02	0.05	0.02	0.03	0.02
Th	4.22	3.11	2.67	2.82	0.65	0.36	1.49	0.47	3.16	0.60
U	1.84	1.14	1.03	1.14	0.36	0.35	0.54	0.22	1.39	0.40
Eu <sub>N</sub> /Eu* <sup>3</sup>	0.68	0.71	0.63	0.61	1.64	1.10	1.03	1.82	0.64	1.06
Zr/Nb	35.2	32.1	39.6	35.9	32.3	43.6	40.0	41.8	41.9	33.0
Hf/Ta	10.5	9.6	11.4	10.8	7.0	13.8	11.6	12.3	14.0	10.0
Zr/Hf	39.5	38.5	39.7	38.6	40.1	33.0	36.4	35.1	38.6	37.3
(Th/Nb) <sub>N</sub> <sup>4</sup>	3.10	2.57	2.51	2.39	2.76	2.90	5.35	3.50	5.75	1.16
Nb/La	0.4	0.5	0.4	0.4	0.4	0.3	0.3	0.3	0.3	0.5

<sup>1</sup> A/CNK = (Al<sub>2</sub>O<sub>3</sub>)/(CaO+Na<sub>2</sub>O+K<sub>2</sub>O) mol%.<sup>2</sup> Mg# = MgO/(MgO+0.505Å~(Fe<sub>2</sub>O<sub>3</sub> Å~0.9+FeO)) assuming that FeO equals to 90% of total Fe-oxide, with FeO and Fe<sub>2</sub>O<sub>3</sub> recalculated from measured values.<sup>3</sup> Eu\* = (Sm<sub>N</sub> Å~ Gd<sub>N</sub>)<sup>1/2</sup>; N: normalization to Chondrites (Sun and McDonough, 1989).<sup>4</sup> n stands for normalization to Primitive Mantle (Sun and McDonough, 1989).

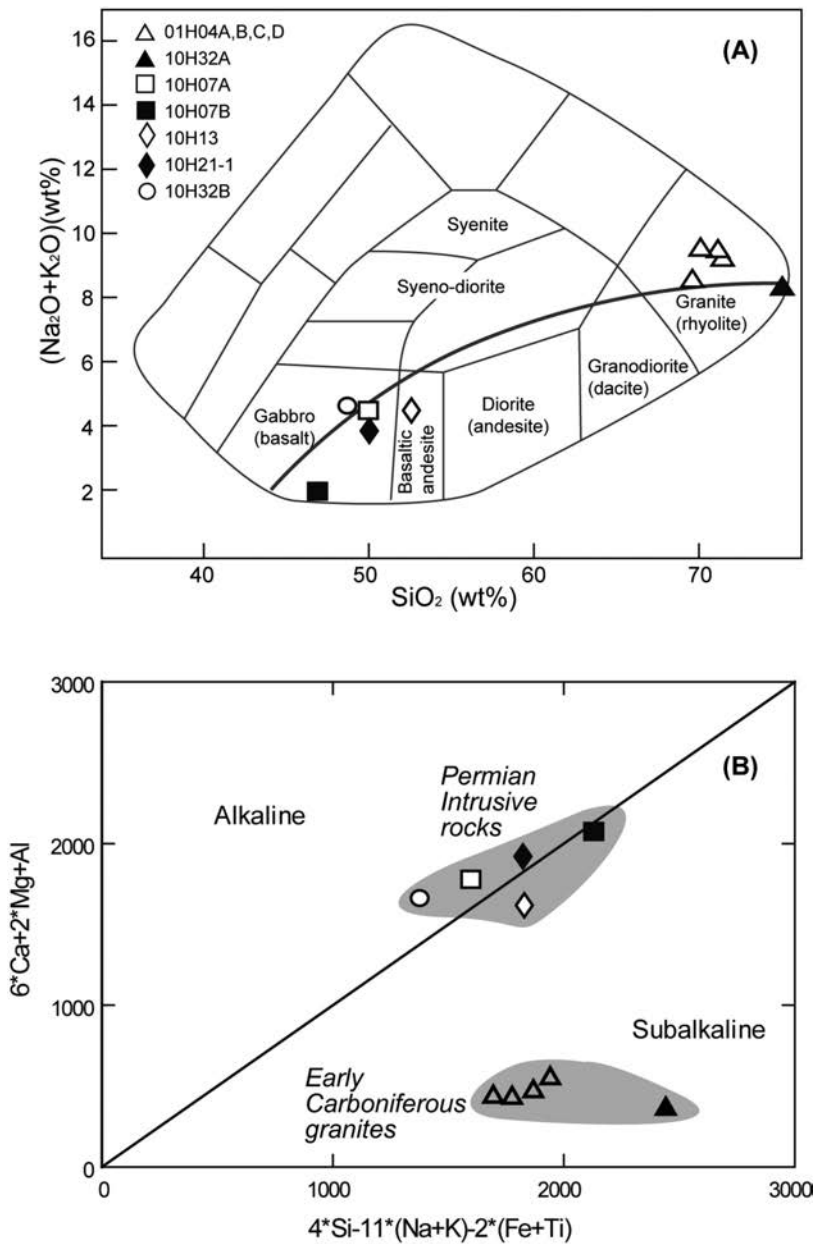


Fig. 9. Geochemical classification diagrams for Carboniferous and Permian intrusive rocks of the eastern Chinese North Tianshan (after Cox and others, 1979; Wilson, 1989).

10H21-1 (fig. 4D). On the multi-element variation diagrams, depletion of Nb and Ta and enrichment of Sr to variable degrees appear on otherwise nearly flat patterns (figs. 11C and 11D). Compared with E-MORB, the analyzed mafic rocks are enriched in Rb, Ba and Th as well. The significance of these geochemical features will be discussed in the following section.

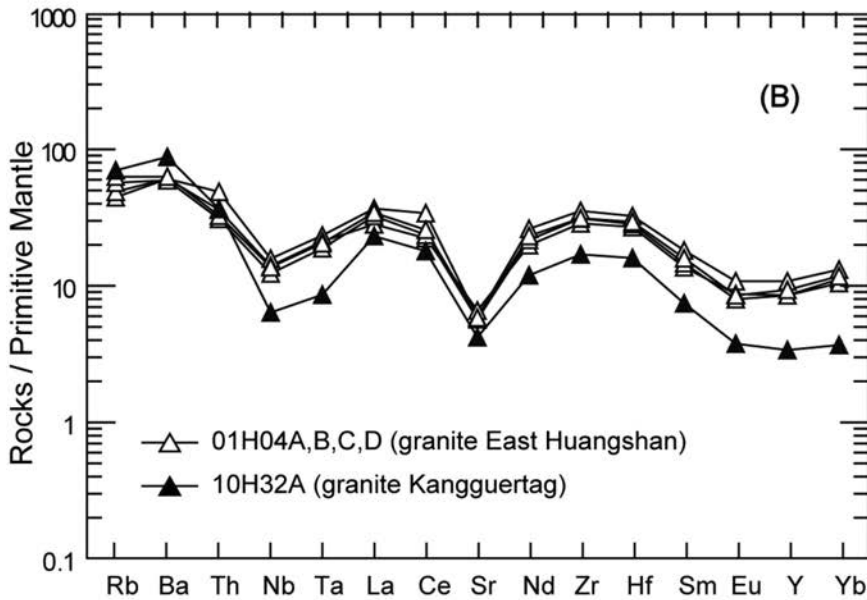
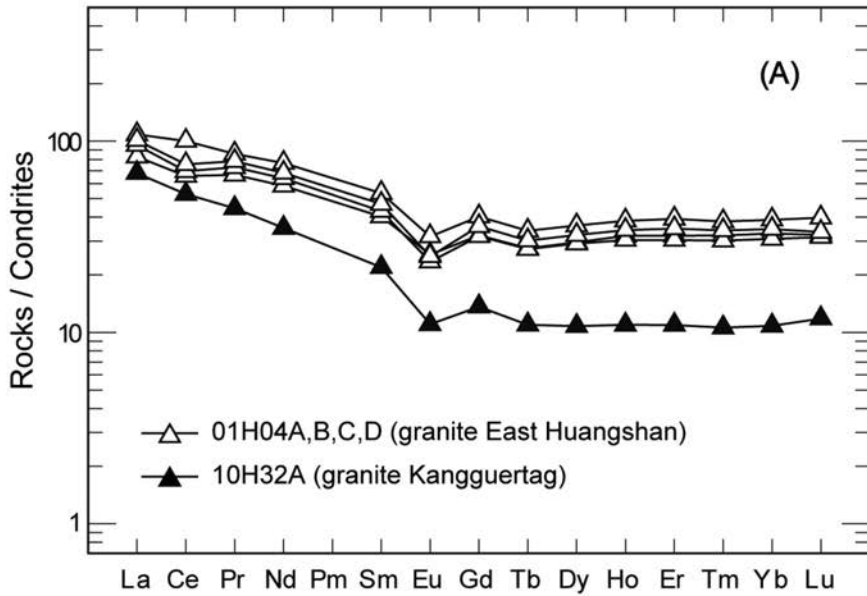


Fig. 10. Chondrite-normalized REE patterns (A) and primitive mantle-normalized multi-element variation diagram (B) for the Carboniferous granites of the eastern Chinese North Tianshan. Normalization values are from Sun and McDonough (1989).

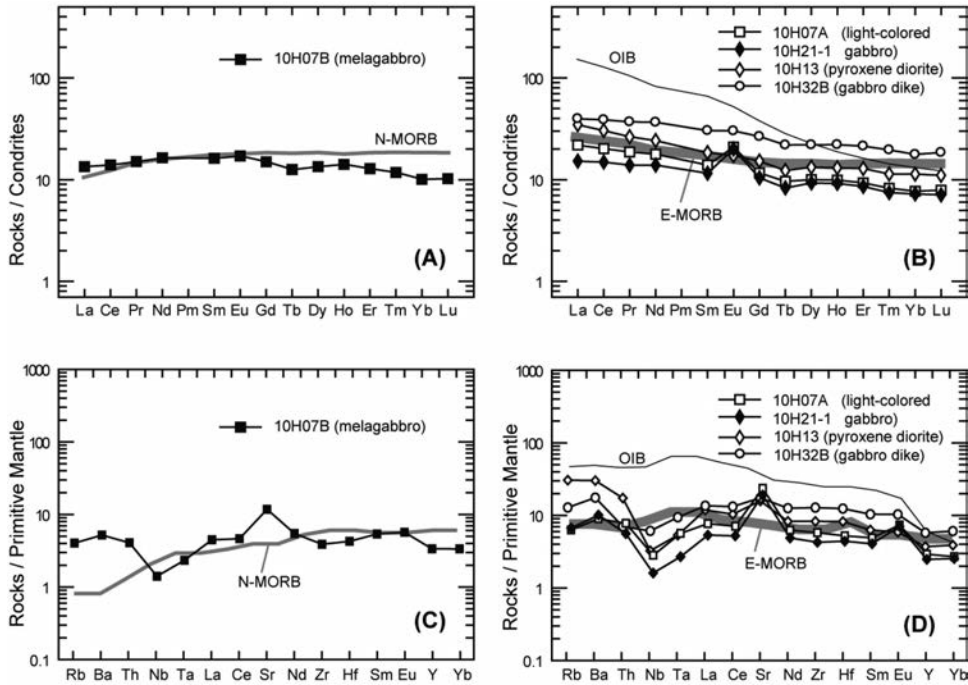


Fig. 11. Chondrite-normalized REE patterns (A & C) and primitive mantle-normalized multi-element variation diagrams (B & D) for the Permian intrusive rocks from the eastern Chinese North Tianshan. Normalization values and reference data for N-MORB, E-MORB and OIB are from Sun and McDonough (1989).

## DISCUSSION

### *Tectonic Settings of the Carboniferous and Permian Intrusive Rocks*

Available geological maps and previous studies suggest that the Carboniferous granitoids in the eastern Chinese North Tianshan are associated with volcanic and volcano-sedimentary rocks (XBGMR, 1993). Most authors consider these magmatic rocks as arc-related (Shu and others, 2000, 2004; Li and others, 2002, 2006a; Sun and others, 2006), whereas, others (Che and others, 1996; Xia and others, 2004, 2008) argue for a continental rift or intraplate environment on the basis of geochemical features. Our data from the early Carboniferous (337-346 Ma) porphyritic biotite granite of the Huangshan area and the K-feldspar granite of the Kangyurtag area reveal Nb and Ta depletion and LILE (Rb, Ba and Th) enrichment (fig. 10), which are geochemical features of calc-alkaline subduction-related magmatic rocks (McCulloch and Gamble, 1991). These features are consistent with those of the Carboniferous mafic and intermediate magmatic rocks in the western Chinese Tianshan (Wang and others, 2009, 2011; Gao and others, 2011). In addition, convergence-related tectonic features were predominant in the eastern Chinese North Tianshan during the Carboniferous (Shu and others, 2000; Xiao and others, 2004; Li and others, 2006a; Charvet and others, 2007, 2011), whereas Carboniferous extensional tectonics were neither documented by sedimentation, nor observed in the field. Therefore, a magmatic arc setting is likely for the studied early Carboniferous granites in the eastern Chinese North Tianshan.

The Permian intrusive rocks show geochemical features that differ obviously from those of the early Carboniferous granites. Two types of mafic intrusions can be

recognized, which are: 1) melagabbro and 2) light-colored gabbro, pyroxene diorite and gabbro dike (figs. 11A and 11C). The melagabbro of the East Huangshan resembles the troctolite and some gabbros of Xiangshan (NW of the Huangshan area) (Xiao and others, 2010b) and gabbro of the Haibaotan area (Li and others, 2006b) (fig. 2). These rocks have total REE abundances of ~0.2 to 2 times those of N-MORB and show bell-shaped REE patterns (figs. 11A and 12A), that suggest origin from a source containing phases that retain LREE and HREE, such as orthopyroxene and garnet (for example, granulite); thus, they probably originated from the melting and differentiation of deep crustal granulite-facies mafic rocks (Garrido and Bodinier, 1999). The light colored gabbro and diorite of the Huangshan area and gabbroic dike of the Kangguertag area have bulk REE contents and flat (E-MORB-like) REE patterns comparable to coeval mafic rocks within or near the Kangguer–Huangshan Shear Zone, including some gabbros in the Xiangshan area (Xiao and others, 2010b), the Baishiquan gabbro (Mao and others, 2006), the Qiatekaer diorite and mafic dikes of Dananhu (Li and others, 2006b) (figs. 11C and 12B). These features suggest an undepleted mantle source with some possible contribution of the asthenosphere for these mafic rocks.

In addition, Permian granites and granitic dikes also occur in the eastern Chinese North Tianshan. Peraluminous granites from Jingerquan (to the east of Huangshan; fig. 2), South of Huangshan and the Tulagen areas (~60 km to the NE of Jingerquan) have been already studied (Tang and others, 2008). They show either a pronounced REE fractionation similar to OIB, or moderately enriched LREE patterns comparable to E-MORB, and their HREE patterns are all flat, like those of calc-alkaline rocks (fig. 12C). Comparison of the REE abundances and distribution patterns of these granites with those of the coeval mafic rocks excludes the possibility of crystallization differentiation; instead, such variable REE distribution patterns indicate that these contemporaneous granites were derived from different magma sources.

The Permian rocks were previously considered to be subduction-related (Xiao and others, 2004; Mao and others, 2006); indeed, Nb and Ta depletion are commonly observed in both depleted and enriched mafic intrusions of the eastern Chinese North Tianshan (figs. 11B and 11D) and also in synchronous felsic intrusions (not shown). Most of these Permian intrusive rocks plot in the fields of volcanic arc granite (VAG) or volcanic arc basalt (VAB) (figs. 13A and 13B) due to their low Nb and Ti contents and Th/Hf (0.3-0.6) and Ta/Th (0.1-0.6) ratios (not shown). However, these geochemical features could also be a result of crustal contamination. For instance, Nb and Ta depletion are commonly observed in intraplate mafic rocks that experienced significant crustal contamination (Xia and others, 2004, 2008). Thus, the moderate Nb and Ta depletions probably indicate that the Permian intrusive rocks were influenced by a low-degree crustal contamination. On the other hand, the metasomatized mantle wedge above a pre-existing (that is Carboniferous) subduction zone may persist for some time and produce magmatic rocks bearing arc-like features in post-collisional or intraplate settings (Liegeois, 1998; Wang and others, 2009). In addition, the geochemical features of the Permian rocks obviously differ from those of typical calc-alkaline series (that is Carboniferous rocks), and the co-existence of depleted and enriched mafic-ultramafic intrusive rocks is unusual for a magmatic arc setting. Taking into account (1) the early Permian extensional tectonics (Li and others, 2006b), (2) associated intraplate magmatism in the Bogda and Haerlike areas (Shu and others, 2011), and (3) the development of an unconformity between the early Permian and younger continental volcanic and sedimentary sequences, it seems that a magmatic-arc setting is not consistent with the overall geological features of the Permian magmatic rocks in the eastern Chinese Tianshan.

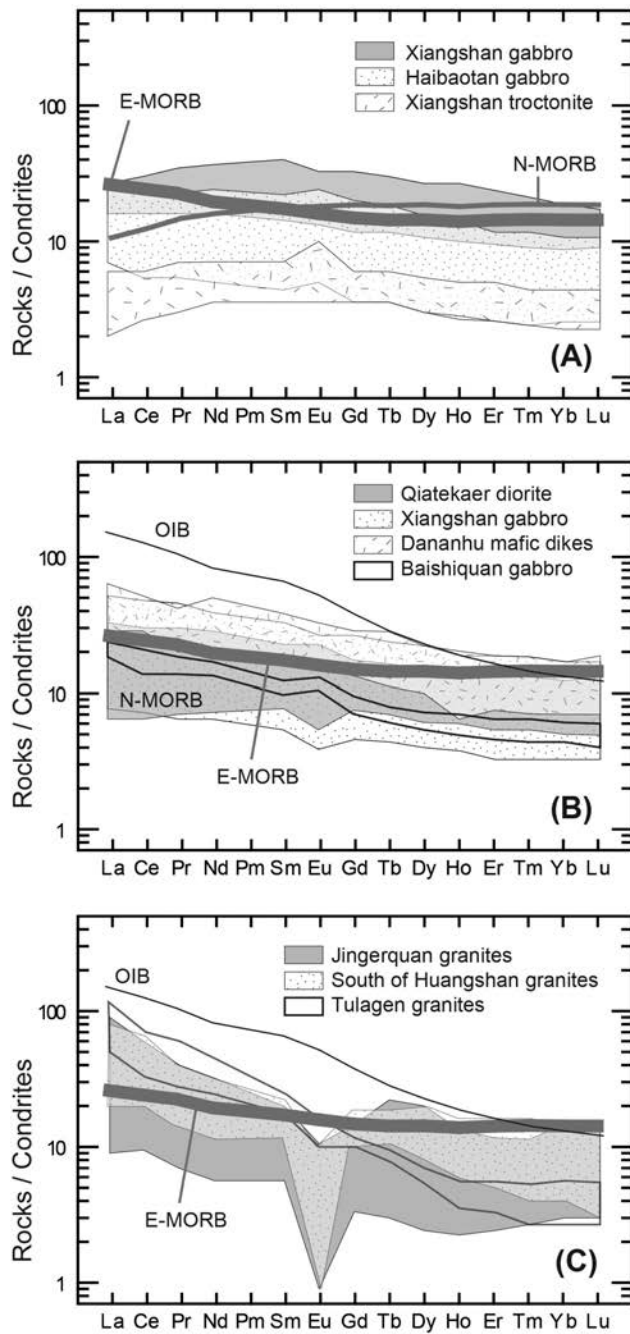


Fig. 12. Chondrite-normalized REE patterns for the Permian mafic and granitic rocks in the eastern Chinese North Tianshan. Data for Qiatekaer diorite, Dananhu dike and Haibaotan gabbro are from Li and others (2006b), those for all granites are from Tang and others (2008); data for Baishiquan gabbro are from Mao and others (2006), and Xiangshan mafic rocks are after Xiao and others (2010b). Normalization values and reference data for N-MORB, E-MORB and OIB are from Sun and McDonough (1989).

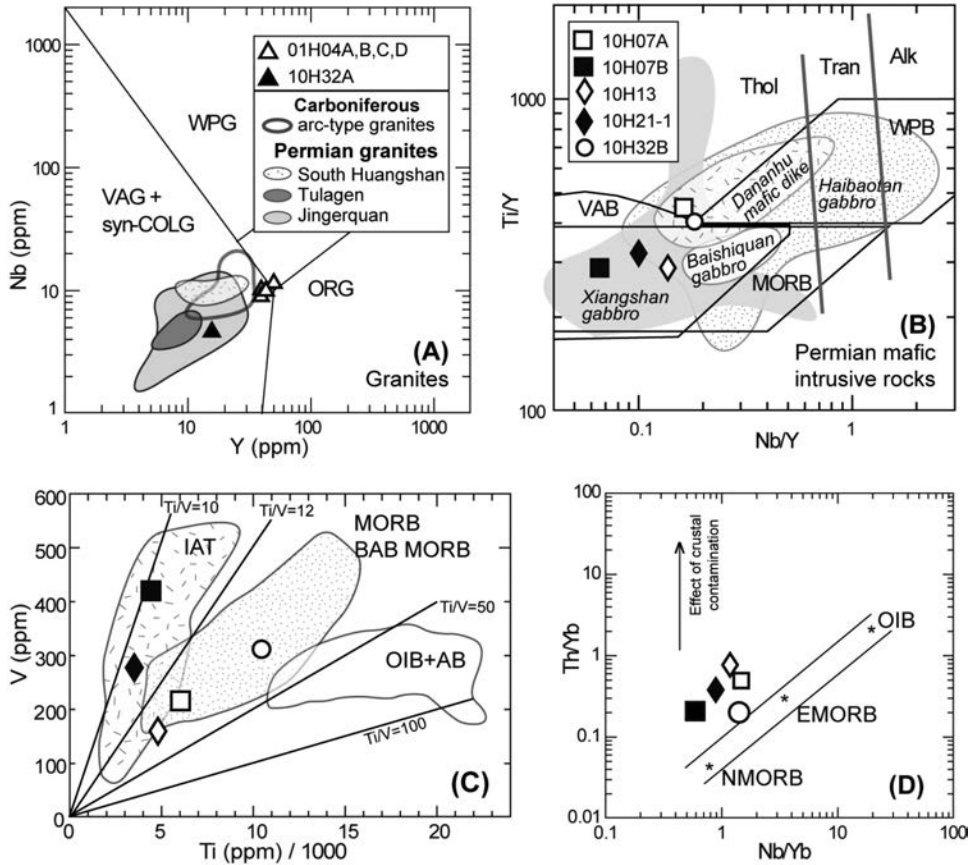


Fig. 13. (A) Y vs Nb discrimination diagram (after Pearce and others, 1984) for the Carboniferous and Permian granitic rocks of the eastern Chinese North Tianshan. Reference data for Carboniferous arc-related granites in the North Tianshan are from Li and others (1998, 2006a); those for Permian granites in the South Huangshan, Tulagen and Jingerquan areas are after Tang and others (2008); (B) Nb/Y vs Ti/Y diagram (Pearce, 1982), (C) Ti/1000 vs V plot (after Shervais, 1982) and (D) Nb/Yb vs Th/Yb diagram (Metcalfe and Shervais, 2008) for the Permian mafic rocks within the Kangguer–Huangshan Shear Zone. See caption of fig. 12 for reference data in (B) that show overlap of different groups of samples.

Significant input of mantle-derived melts is another important feature of Permian magmatic rocks (figs. 13C and 13D), and this is indicated by the high  $\epsilon_{Nd}(t)$  values (+5.5 to +7.2) of peraluminous granites (Tang and others, 2008), which show a weak influence of continental crust-derived melts. Both mafic lower crust and undepleted mantle were involved in the generation of Permian mafic and ultramafic rocks. A mantle origin is also inferred from the association of mafic-ultramafic intrusive complexes with prominent magmatic Ni-Cu ore deposits (Zhou and others, 2004; Han and others, 2006; Chai and others, 2008; Mao and others, 2008). On the basis of these features, together with zircon hafnium- and oxygen-isotope data, Su and others (2011) linked the mafic-ultramafic complexes of the eastern Chinese Tianshan with OIB-type flood basalts in the SW Tarim Basin (Chen and others, 1997; Zhou and others, 2009) and further proposed a model of a mantle plume rooted beneath the eastern Chinese Tianshan and Beishan belts. However, except for consistent mantle sources of mafic-ultramafic rocks, this model does not include any other geological evidence. Actually,

the linear distribution of Permian magmatic rocks along an E-W trending belt and the predominant SE-NW orientation of mafic dikes are not consistent with the general configuration of a mantle plume.

In summary, the Permian magmatic rocks imply variable sources that comprise mantle wedge-like, sub-crustal (granulitic) and asthenosphere-like components. Neither a magmatic arc nor a mantle plume fits with the field and regional geological evidence. It is important to keep in mind that geochemical diagrams only discriminate sources/magma forming processes, but not directly geodynamic/tectonic settings, and the discrimination of these needs to take into account other geological features (sedimentary, tectonic *et cetera*). Thus, a tectonic setting cannot be reliably determined from the overlapping fields and complicated plot trends (fig. 13) of different rock-types with the same age (intrusive complex). Instead, such magmatic complexes were probably produced by a mixture in variable degrees of different sources that co-existed in a specific region. In this case, any given element depletion or enrichment may have resulted from different degrees of mixing levels rather than reflecting one single origin. Despite this complexity, the coexistence and interaction of subduction-related material, magmas from homogeneous mantle sources, and magma of sub-crustal origin, are diagnostic of post-collisional magmatism (Liegeois, 1998) and are significant features of Permian magmatic activity in the eastern Chinese North Tianshan. Thus, a post-collisional setting as proposed by some previous authors (Li and others, 2006b; Wang and others, 2009; Shu and others, 2011) fits well with the general regional tectonic evolution and is a plausible tectonic environment for the Permian magmatism.

On the other hand, the Permian magmatic rocks with multiple mantle sources could also be produced in a ridge-subduction system as has recently been proposed for the latest Carboniferous to early Permian magmatic rocks in the West Junggar (Geng and others, 2009; Tang and others, 2010, 2012a, 2012b; Ma and others, 2012). Indeed, a slab window in the ridge-subduction system may provide space for upwelling of deep mantle, which interacts with the mantle wedge above the subducting slab to form complex magmas with variable sources. However, if such a model is the case in the eastern Chinese Tianshan, it means that (1) the subduction of oceanic lithosphere continued at least up to the end of early Permian, and (2) closure of the oceanic basin and subsequent collision should have occurred later than early Permian. Nevertheless, previous studies (Ma and others, 1997; Shu and others, 2000; Han and others, 2004, 2011; Li and others, 2006b; Charvet and others, 2007, 2011) indicate that subduction tectonics in the eastern Chinese North Tianshan had terminated by the beginning of the early Permian. This conclusion is based on sedimentary and structural data including (a) regionally unconformable middle-upper Permian continental and fluvial deposits, (b) the absence of regional metamorphism or subduction/collision-related convergent deformation since early Permian, except for localized ductile strike-slip shear zones. Thus, although ridge subduction could be a potential interpretation for the production of a wide variety of magmas, it does not fit with the other geological evidence, and therefore becomes unlikely as an explanation for the tectonic setting of the Permian magmatism in the eastern Chinese Tianshan.

*Synkinematic character of the Permian Intrusive Rocks and Relation to the Kangguer–Huangshan Shear Zone*

The Kangguer–Huangshan Shear Zone is a regional-scale shear zone that can be recognized from satellite images and geophysical maps. Intense ductile deformation has been already described from this mega-shear zone. Although Xu and others (2003) proposed a coaxial strain regime, most authors consider it as a polyphase shear zone, in which earlier convergence (Carboniferous to earliest Permian) and later (Permian) transcurrent tectonics are superimposed (Shu and others, 1999; Laurent-Charvet and

others, 2002, 2003; Li and others, 2002, 2006b; Wang and others, 2008c). Our observations and structural analysis suggest that the bulk structure of the Kangguer–Huangshan Shear Zone resulted from dextral strike-slip shearing during the Permian (Branquet and others, 2012) with localized thrusting or normal faulting in response to local transpression or transtension, respectively.

Lithology is a dominating factor in rock deformation and controls the strain intensity and the ductility of rocks at a given stress and crustal level (corresponding temperature) (Gapais and others, 2005). In the Kangguer–Huangshan Shear Zone, “soft” Carboniferous volcano-sedimentary rocks have been strongly sheared, whereas relatively stronger granitic rocks of early Carboniferous age are free of ductile deformation and only cross-cut and offset by brittle strike-slip faults. This means that the deformation observed at the present surface level occurred at relatively low temperature, which is consistent with the development of greenschist-facies metamorphism in slaty country rocks.

In contrast, the Permian intrusive rocks show various strain fabrics, including mylonitic foliation/lineation in the marginal facies of the East Huangshan mafic-ultramafic complex, and shape-preferred orientation of quartz and biotite crystals in the tongue-shaped K-feldspar granite of the Kangguertag area. These fabrics reflect the rheological behavior of a crystal-bearing magma, suggesting that magma ascent, emplacement and cooling/crystallization occurred in a regional strain field (Petford, 2003). Considering that the fabrics in the Permian intrusive rocks are consistent with that of the Kangguer–Huangshan Shear Zone as established by Branquet and others (2012), it is reasonable to conclude that these fabrics result from syn- and/or late magmatic deformation and correspond to synkinematic pluton emplacement associated with regional-scale dextral transcurrent tectonics. It is necessary to point out that the deformation fabrics in the Permian rocks along the shear zone are distinct from the structures of a subduction/collisional belt. Thus, the deformation of Permian rocks cannot be considered as evidence for Permian or post-Permian subduction or accretionary events.

Apart from structural evidence, geochronological constraints also reveal the syn-tectonic character of the Permian intrusive rocks. Our zircon age data suggest that the mafic-ultramafic complex of East Huangshan intruded in the interval 267 to 275 Ma (table 1), and this is consistent with the age of an olivine norite in this complex (Han and others, 2004). Previous studies provided more age constraints (fig. 2; table 4) on the Permian intrusive rocks within and off the Kangguer–Huangshan Shear Zone. Combined with our new data (table 1), it can be summarized that mafic intrusions were emplaced during 269 to 287 Ma, the intermediate intrusions were emplaced at 252 to 271 Ma, and the felsic plutons intruded from 260 Ma to 297 Ma. The available literature reports thermo-chronological results on strongly deformed or synkinematic plutonic rocks, metamorphosed volcano-sedimentary rocks and associated gold deposits along the Kangguertag–Juoloutag and Huangshan–Jingerquan dextral shear zone (table 5). These data indicate a main phase of ductile shearing from ~290 to ~250 Ma and subsequent cooling until ~240 to ~230 Ma. Similar thermal events were documented in the Main Tianshan Shear Zone (Shu and others, 1999; Laurent-Charvet and others, 2002, 2003) and in the Nalati Fault and North Tianshan Fault of the western Chinese Tianshan (Yin and Nie, 1996; de Jong and others, 2009; Wang and others, 2010).

These age data clearly show that the intrusion of Permian magmatic rocks and dextral ductile shearing occurred synchronously. On the other hand, although the age range of intermediate intrusions seems younger than that of mafic and felsic rocks, no regular evolution of the different kinds of magmatic rocks can be recognized, and they show significant overlap both in time and space (fig. 2; table 4). This phenomenon is

TABLE 4

*Summary of published zircon ages of mafic, intermediate and felsic intrusions in the Kangguer–Huangshan Shear Zone*

Location	Coordinate	Rock type	Age (Ma)	Reference
<b>Mafic intrusions</b>				
<i>Haibaotan ringshaped complex</i>		Altered gabbro	269.2 ± 3.2	Li and others, 2006b
		Serpentinized troctolite	282~287	Li and others, 2006b
<i>Qiatekartag complex</i>		Altered gabbro	277 ± 1.6	Li and others, 2006b
		Diabase dike intruding granite	271~280	Li and others, 2006b
<i>Baishiquan Mine East Huangshan</i>		Gabbro	281.2 ± 0.9	Mao and others, 2006
		Olivine norite	274 ± 3	Han and others, 2004
<b>Intermediate intrusions</b>				
<i>Shuangchagou pluton</i>	N42°07'49.8" E94°52'36.8"	Granodiorite	252.4 ± 2.9	Zhou and others, 2010
<i>Keziertag pluton</i>	N42°07' E91°33'	Fine-grained granodiorite	271.6 ± 1.6	Li and others, 2006c
<i>Caixiashan East</i>	N42°08' E91°54'	Quartz diorite	267.8 ± 1.6	Ren and others, 2006
<i>Longdong, Kumutag</i>		Quartz diorite	261	Li and others, 2007
<b>Felsic intrusions</b>				
<i>Dikaner pluton, NE</i>	N42°23'09.2" E89°57'03.3"	Porphyritic K-granite	288 ± 2.5	Zhou and others, 2010
<i>Xiaorequanzi Baishandong pluton, Baishan Mine</i>	N42°29'53.5" E95°56'37.7"	Granite	284.5 ± 4.5	Zhou and others, 2010
<i>Guandao pluton, NE Aqishan</i>	N42°09'20.3" E90°32'55.8"	Granitic porphyry	284.1 ± 5.8	Zhou and others, 2010
<i>Hongshi pluton, NW Kangguer</i>	N42°09'20.2" E90°48'10.2"	Granite	282.7 ± 4.2	Zhou and others, 2010
<i>Longdong pluton, West Yamansu</i>	N41°59'02.2" E93°14'11.4"	Monzogranite <sup>2</sup>	76.2 ± 2.5	Zhou and others, 2010
<i>Duotoushan pluton, Caixiashan Mine</i>	N41°43'47.7" E91°22'33.7"	K-granite	271.7 ± 5.5	Zhou and others, 2010
<i>Huangshan pluton, S East Huangshan</i>	N42°08'48.0" E94°39'18.1"	K-granite	288 ± 17	Zhou and others, 2010
<i>South Huangshan Tulagen pluton</i>		Muscovite granite Two mica granite	259.9 ± 1.4 275.4 ± 8.3	Tang and others, 2008 Tang and others, 2008
<i>Shalondong, Kumutag Weiquan Mine, West of Tuwu</i>		Monzogranite Granite	293 ± 6 297 ± 3	Zhang and others, 2006 Wang and others, 2005

also observed in the western Chinese Tianshan (Wang and others, 2009) and in the Transbaikal Region of Central Asia (Litvinovsky and others, 2011), and is linked with multiple-source magmatism. In the Chinese Central and Western Tianshan, Permian intrusive rocks are located along major strike-slip shear zones and show similar shapes and synkinematic fabrics (Wang and others, 2009).

Considering that (1) large-scale strike-slip shearing occurred in the Kangguer–Huangshan zone, (2) there are synchronous Permian magmatic intrusions with synkinematic ductile deformation, (3) multiple mantle sources with subduction-inherited and lower crust components are implied, and (4) a post-collisional setting for the Permian intrusions is likely, we propose that synkinematic plutonism controlled by a mega-shear zone occurred in a post-collisional environment, as shown by Wang and others (2009) and Branquet and others (2012). In this model, the Kangguer–

TABLE 5

*Compilation of published geochronological results for the Kangguer–Huangshan Shear Zone*

Location	Rock	Material	Method	Age (Ma)	Reference
Jingerquan	Mylonitic granite	Whole rock	Rb-Sr	260.5	Yang, 1998 ms
Aqishan	Granitic porphyry	K-feldspar	Ar-Ar	278.8 ± 2.1	Chen and others, 2005
Kangguertag	Muscovite chlorite mylonite	Muscovite	Ar-Ar	283.7 ± 2.4	Chen and others, 2005
	mylonitic quartz keratophyre	Plagioclase	Ar-Ar	256.1 ± 4.1	
Gold deposits of Kangguertag	Gold ore	Sericite	Ar-Ar	256.9 ± 4.4	Chen and others, 2005
	mylonitic quartz keratophyre	Whole rock	Ar-Ar	262.2 ± 1.5	
	Phyllonite	Whole rock	Ar-Ar	261.5 ± 1.2	
	mylonitic volcaniclastic rock	Whole rock	Ar-Ar	262.9 ± 1.4	
	granitic mylonite	Whole rock	Ar-Ar	260.1 ± 1.8	
Gold deposit of Kangguertag	Gold-bearing quartz fluid inclusion	Whole rock	Rb-Sr	282 ± 5	Li and others, 1998
Gold deposit of Kangguertag	Sulphide	Sulphide	Sm-Nd	290 ± 7	Wang and others, 2006b
Kangguertag	Altered andesite	Whole rock	Rb-Sr	290 ± 5	
Jueluotag	Amphibolite	Amphibole	Ar-Ar	276	Wang and others, 2002
Jueluotag- Kangguertag	Tongue-shaped granite	Hornblende	Ar-Ar	272-277	Wang and others, 2008c
		Biotite	Ar-Ar	254-261	
		K-feldspar	Ar-Ar	226-241	
	Mylonitic granite Dioritic porphyry Granite	K-feldspar	Ar-Ar	230-231	
		Plagioclase	Ar-Ar	268 ± 3	
		Biotite	Ar-Ar	252 ± 2	

Huangshan Shear Zone provided ascent channels for the mafic/ultramafic to felsic magmas derived from sources that include depleted and undepleted (or enriched) mantle, fluids released from an earlier subducted slab and partially melted lower continental crust. The undepleted or enriched magmas could be generated by upwelling of deep mantle along a slab window produced by slab break-off (Wang and others, 2009; Zhang and others, 2012); or local extreme crustal thinning and asthenosphere uplift, without the necessity for a mantle plume, which is not supported by geological or structural data. This model may also account for the emplacement of complex magmatic suites controlled by transcurrent tectonics in other regions of Central Asia (Pirajno, 2010; Litvinovsky and others, 2011; Zhang and others, 2012).

#### *General Implications for Regional Tectonic Evolution*

Our study suggests that the early Carboniferous magmatic rocks in the eastern Chinese North Tianshan belong to a typical calc-alkaline series and most likely represent a magmatic arc related to the subduction of the Paleo-Junggar Ocean. The arc-related magmatism continued up to late Carboniferous and is characterized by I-type granitoids associated with coeval basalt-andesite-rhyolite volcanic series and interlayered sedimentary rocks (Ma and others, 1997; Li and others, 2002, 2006a; Wu and others, 2008; Zhang and others, 2010; Zhou and others, 2010). The occurrence of this Carboniferous magmatic arc is consistent with the views of previous authors (Shu and others, 2000; Li and others, 2007, 2011) who mainly considered the regional convergent and accretionary tectonics.

In contrast, Permian intrusions show distinct geochemical features that reveal a significant change of magma sources and tectonic setting as well. Permian tectonics are characterized by large-scale dextral motion along the Kangguer–Huangshan Shear Zone and also in the Main Tianshan Shear Zone. Dominant strike-slip shearing and homogenous mantle sources with involvement of subduction-related components in the synkinematic magmatic rocks suggest a post-collisional setting during the Permian period, following the Carboniferous subduction and accretion. The transition from convergent to transcurrent tectonics probably occurred in the earliest Permian (Wang and others, 2009; Shu and others, 2011; Zhang and others, 2012). Since the Chinese Tianshan belt is located in the southernmost part of the CAOB, this tectonic transition suggests that the building of the CAOB and its final amalgamation with the Tarim terminated at the Permian-Carboniferous boundary. A regional angular unconformity and accumulation of middle to upper Permian continental red-beds (Shu and others, 2011) post-date the peak stage (early Permian) of ultramafic and mafic magmatism in the region, and thus do not support a plume-induced crustal uplift (Xia and others, 2004, 2008; Su and others, 2011).

The nature of the basement in the eastern Chinese North Tianshan is an issue for discussion since there are no exposed rocks older than Late Devonian. Some authors have linked the eastern Chinese North Tianshan with the Yili block in the west to define the Yili-North Tianshan that represents a late Paleozoic arc emplaced upon a similar Precambrian basement (Wang and others, 2008a; Charvet and others, 2011), but classically it is considered as an arc terrain with unknown basement (Li and others, 2002; Xiao and others, 2004). Our new age data on the Carboniferous and Permian intrusive rocks in the Kangguer–Huangshan Shear Zone include inherited early to mid-Paleozoic zircons ( $\sim 380\text{--}390$  Ma,  $\sim 450\text{--}470$  Ma), and Proterozoic zircons as well ( $\sim 1.3$  Ga, 1.6 Ga, 1.9 Ga and 2.2 Ga) (table 1). Although the sources and significance of these Proterozoic zircons are uncertain, they suggest the existence of old crust beneath the eastern Chinese North Tianshan. Such old crust is well documented in the Kyrgyz North Tianshan (Kröner and others, 2013, 2014). Further study is necessary to determine whether these zircons represent the *in-situ* crystalline basement of the late Paleozoic magmatic arc or were simply recycled into the late Paleozoic sediments and incorporated in Permian granitoids.

#### CONCLUSIONS

1. Carboniferous granitic rocks in the Huangshan and Kangguertag areas formed at  $338 \pm 4$  Ma and  $347 \pm 2$  Ma, respectively. They show porphyritic textures and massive structures without significant ductile deformation. They belong to a typical calc-alkaline series and may be related to the late Paleozoic magmatic arc of the Chinese North Tianshan.

2. Permian intrusive rocks are well developed within or close to the Kangguer–Huangshan Shear Zone and display synkinematic emplacement features. These Permian magmatic rocks were emplaced synchronously with the tectonic activity on the Kangguer–Huangshan Shear Zone.

3. Geochemical data suggest that the Permian magmatic rocks differ from the Carboniferous arc-related granitic rocks. REE features of the Permian intrusive rocks indicate that they were derived from either enriched/undepleted or depleted magmas with involvement of subduction-related components. Such important mantle input in the Permian magmatic rocks indicates significant crust growth in the Chinese North Tianshan.

4. It is suggested that the Permian intrusive rocks of the Kangguer–Huangshan Shear Zone most likely formed in a post-collisional/orogenic transcurrent setting that followed Carboniferous subduction and accretion. Owing to their synkinematic emplace-

ment features, we suggest that large-scale dextral tectonics probably controlled the intrusion of the Permian plutons.

#### ACKNOWLEDGMENTS

We thank Dr. G. Shellnutt and the other Guest Editors for organizing this special issue honoring the research career of Professor Bor-ming Jahn. We appreciate the kind help of Professors B. L. Wang, H. D. Ma and Ms. L. Wen during the field work. Dr. G. R. Li, Mr. F. Wang and Mr. K. S. Li participated in parts of the field work and analysis of zircons. We also thank Professor W. L. Griffin, Professor J. P. Zheng, and Professor A. Kröner for their comments and constructive suggestions that helped us a lot with improving our manuscript. Professor W. L. Griffin and Professor A. Kröner improved the English. This study was co-sponsored by the National Nature Science Foundation of China (41390445, 41172197, 41222019, 40802043), the Foundation for the Author of National Excellent Doctoral Dissertation of PR China (FANEDD, No. 201130), the Fok Ying Tung Education Foundation (131016), the Scientific Research Foundation for Returned Overseas Chinese Scholars, State Education Ministry of China, and the Fundamental Research Funds for the Central Universities (to B. Wang). BM Jahn acknowledges the support of the National Research Council (Taiwan) through grants NSC-100-2116-M-002-024 and NSC-101-2116-M-002-003. This study is also a contribution to IGCP-592 Project.

#### REFERENCES

- Allen, M. B., Windley, B. F., and Zhang, C., 1993, Paleozoic collisional tectonics and magmatism of the Chinese Tien Shan, Central Asia: *Tectonophysics*, v. 220, n. 1–4, p. 89–115, [http://dx.doi.org/10.1016/0040-1951\(93\)90225-9](http://dx.doi.org/10.1016/0040-1951(93)90225-9)
- Allen, M. B., Sengör, A. M. C., and Natal'in, B. A., 1995, Junggar, Turfan and Alakol basins as Late Permian to Early Triassic extensional structures in a sinistral shear zone in the Altaid orogenic collage, Central Asia: *Journal of the Geological Society, London*, v. 152, n. 2, p. 327–338, <http://dx.doi.org/10.1144/gsjgs.152.2.0327>
- Andersen, T., 2002, Correction of common lead in U–Pb analyses that do not report  $^{204}\text{Pb}$ : *Chemical Geology*, v. 192, n. 1–2, p. 59–79, [http://dx.doi.org/10.1016/S0009-2541\(02\)00195-X](http://dx.doi.org/10.1016/S0009-2541(02)00195-X)
- Avouac, J. P., Tapponnier, P., Bai, M., You, H., and Wang, G., 1993, Active thrusting and folding along the northern Tien Shan and Late Cenozoic rotation of the Tarim relative to Dzungaria and Kazakhstan: *Journal of Geophysical Research-Solid Earth*, v. 98(B4), p. 6755–6804, <http://dx.doi.org/10.1029/92JB01963>
- Black, L. P., Kamo, S. L., Allen, C. M., Aleinikoff, J. N., Davis, D. W., Korsch, R. J., and Foudoulis, C., 2003, TEMORA 1: a new zircon standard for Phanerozoic U–Pb geochronology: *Chemical Geology*, v. 200, n. 1–2, p. 155–170, [http://dx.doi.org/10.1016/S0009-2541\(03\)00165-7](http://dx.doi.org/10.1016/S0009-2541(03)00165-7)
- Branquet, Y., Gumiaux, C., Sizaret, S., Barbanson, L., Wang, B., Cluzel, D., Li, G. R., and Delaunay, A., 2012, Synkinematic mafic/ultramafic sheeted intrusions: Emplacement mechanism and strain restoration of the Permian Huangshan Ni–Cu ore belt (Eastern Tianshan, NW China): *Journal of Asian Earth Sciences*, v. 56, p. 240–257, <http://dx.doi.org/10.1016/j.jseas.2012.05.021>
- Buslov, M. M., 2011, Tectonics and geodynamics of the Central Asian Foldbelt: the role of Late Paleozoic large-amplitude strike-slip faults: *Russian Geology and Geophysics*, v. 52, n. 1, p. 52–71, <http://dx.doi.org/10.1016/j.rgg.2010.12.005>
- Chai, F. M., Zhang, Z. C., Mao, J. W., Dong, L. H., Zhang, Z. H., and Wu, H., 2008, Geology, petrology and geochemistry of the Baishiquan Ni–Cu-bearing mafic–ultramafic intrusions in Xinjiang, NW China: Implications for tectonics and genesis of ores: *Journal of Asian Earth Sciences*, v. 32, n. 2–4, p. 218–235, <http://dx.doi.org/10.1016/j.jseas.2007.10.014>
- Charvet, J., Shu, L. S., and Laurent-Charvet, S., 2007, Paleozoic structural and geodynamic evolution of eastern Tianshan (NW China): Welding of the Tarim and Junggar plates: *Episodes*, v. 30, n. 3, p. 162–186.
- Charvet, J., Shu, L. S., Laurent-Charvet, S., Wang, B., Faure, M., Cluzel, D., Chen, Y., and de Jong, K., 2011, Palaeozoic tectonic evolution of the Tianshan belt, NW China: *Science in China (Earth Sciences)*, v. 54, n. 2, p. 166–184, <http://dx.doi.org/10.1007/s11430-010-4138-1>
- Che, Z. C., Liu, L., Liu, H. F., and Luo, J. H., 1996, Review on the ancient Yili rift, Xinjiang, China: *Acta Petrologica Sinica*, v. 12, n. 3, p. 478–490 (in Chinese with English abstract).
- Chen, C. M., Lu, H. F., Jia, D., Cai, D. S., and Wu, S. M., 1999, Closing history of the southern Tianshan oceanic basin, western China: an oblique collisional orogeny: *Tectonophysics*, v. 302, n. 1–2, p. 23–40, [http://dx.doi.org/10.1016/S0040-1951\(98\)00273-X](http://dx.doi.org/10.1016/S0040-1951(98)00273-X)
- Chen, H. L., Yang, S. F., and Dong, C. W., 1997, The discovery of early Permian basic rock belt in the Tarim basin and its tectonic meaning: *Geochemica*, v. 26, p. 77–87 (in Chinese with English abstract).

- Chen, W., Sun, S., Zhang, Y., Xiao, W. J., Wang, Y. T., Wang, Q. L., Jiang, L. F., and Yang, J. T., 2005,  $^{40}\text{Ar}$ - $^{39}\text{Ar}$  geochronology of the Qiugemingtashi-Huangshan ductile shear zone in east Tianshan, Xinjiang, NW China: *Acta Geologica Sinica*, v. 79, n. 6, p. 790–804 (in Chinese with English abstract).
- Choulet, F., Chen, Y., Wang, B., Faure, M., Cluzel, D., Charvet, J., Lin, W., and Xu, B., 2011, Late Paleozoic paleogeographic reconstruction of Western Central Asia based upon paleomagnetic data and its geodynamic implications: *Journal of Asian Earth Sciences*, v. 42, n. 5, p. 867–884, <http://dx.doi.org/10.1016/j.jseas.2010.07.011>
- Coleman, R. G., 1989, Continental growth of northwest China: *Tectonics*, v. 8, n. 3, p. 621–635, <http://dx.doi.org/10.1029/TC008i003p00621>
- Compston, W., Williams, I. S., Kirschvink, J. L., Zhang, Z. C., and Ma, G. G., 1992, Zircon U–Pb ages for the Early Cambrian time scale: *Journal of the Geological Society, London*, v. 149, n. 2, p. 171–184, <http://dx.doi.org/10.1144/gsjgs.149.2.0171>
- Corfu, F., Hanchar, J. M., Hoskin, P. W. O., and Kinny, P., 2003, Atlas of zircon textures: Reviews in Mineralogy and Geochemistry, v. 53, n. 1, p. 469–500, <http://dx.doi.org/10.2113/0530469>
- Couture, R. A., Smith, M. S., Dymek, R. F., 1993, X-ray fluorescence analysis of silicate rocks using fused glass discs and a side-window Rh source tube: accuracy, precision and reproducibility: *Chemical Geology*, v. 110, n. 4, p. 315–328, [http://dx.doi.org/10.1016/0009-2541\(93\)90326-E](http://dx.doi.org/10.1016/0009-2541(93)90326-E)
- Cox, K. G., Bell, J. D., and Pankhurst, R. J., 1979, *The Interpretation of Igneous Rocks*: London, George, Allen and Unwin, 450 p.
- De Jong, K., Wang, B., Faure, M., Shu, L. S., Cluzel, D., Charvet, J., Ruffet, G., and Chen, Y., 2009, New  $^{40}\text{Ar}$ - $^{39}\text{Ar}$  age constraints on the Late Palaeozoic tectonic evolution of the western Tianshan (Xinjiang, northwestern China), with emphasis on Permian fluid ingress: *International Journal of Earth Sciences*, v. 98, n. 6, p. 1239–1258, <http://dx.doi.org/10.1007/s00531-008-0338-8>
- Gao, J., Li, M. S., Xiao, X. C., Tang, Y. Q., and He, G. Q., 1998, Paleozoic tectonic evolution of the Tianshan Orogen, northern China: *Tectonophysics*, v. 287, n. 1–4, p. 213–231, [http://dx.doi.org/10.1016/S0040-1951\(98\)80070-X](http://dx.doi.org/10.1016/S0040-1951(98)80070-X)
- Gao, J., Long, L. L., Klemm, R., Qian, Q., Liu, D. Y., Xiong, X. M., Su, W., Liu, W., Wang, Y. T., and Yang, F. Q., 2009, Tectonic evolution of the South Tianshan orogen and adjacent regions, NWChina: geochemical and age constraints of granitoid rocks: *International Journal of Earth Sciences*, v. 98, n. 6, p. 1221–1238, <http://dx.doi.org/10.1007/s00531-008-0370-8>
- Gao, J., Klemm, R., Qian, Q., Zhang, X., Li, J. L., Jiang, T., and Yang, Y. Q., 2011, The collision between the Yili and Tarim blocks of the Southwestern Altai: Geochemical and age constraints of a leucogranite dike crosscutting the HP–LT metamorphic belt in the Chinese Tianshan Orogen: *Tectonophysics*, v. 499, n. 1–4, p. 118–131, <http://dx.doi.org/10.1016/j.tecto.2011.01.001>
- Gao, J. F., Lu, J. J., Lai, M. Y., Lin, Y. P., and Pu, W., 2003, Analysis of trace elements in rock samples using HR-ICPMS: *Journal of Nanjing University (Natural Sciences)*, v. 39, n. 6, p. 844–850 (in Chinese with English abstract).
- Gapais, D., Brun, J. P., and Cobbold, P. R., 2005, *Deformation Mechanisms, Rheology and Tectonics: from Minerals to the Lithosphere*: Geological Society, London, Special Publications, 243 p.
- Garrido, C. J., and Bodinier, J. L., 1999, Diversity of mafic rocks in the Ronda peridotite: evidence for pervasive melt-rock reaction during heating of subcontinental lithosphere by upwelling asthenosphere: *Journal of Petrology*, v. 40, n. 5, p. 729–754, <http://dx.doi.org/10.1093/ptro/40.5.729>
- Geng, H. Y., Sun, M., Yuan, C., Xiao, W. J., Xian, W. S., Zhao, G. C., Zhang, L. F., Wong, K., and Wu, F. Y., 2009, Geochemical, Sr–Nd and zircon U–Pb–Hf isotopic studies of Late Carboniferous magmatism in the West Junggar, Xinjiang: Implications for ridge subduction?: *Chemical Geology*, v. 266, n. 3–4, p. 364–389, <http://dx.doi.org/10.1016/j.chemgeo.2009.07.001>
- Guo, J., Shu, L. S., Charvet, J., Laurent-Charvet, S., and Sun, S. W., 2002, Geochemical features of the two early paleozoic ophiolitic zones and volcanic rocks in the central-southern Tianshan Region, Xinjiang: *Chinese Journal of Geochemistry*, v. 21, n. 4, p. 308–321.
- Han, B. F., Ji, J. Q., Song, B., Chen, L. H., and Li, Z. H., 2004, SHRIMP zircon U–Pb ages of Kalatongke No. 1 and Huangshandong Cu–Ni-bearing mafic–ultramafic complexes, North Xinjiang, and geological implications: *Chinese Science Bulletin*, v. 49, n. 22, p. 2424–2429, <http://csb.scichina.com:8080/kxtbe/EN/10.1360/04wd0163>
- Han, B. F., He, G. Q., Wang, X. C., and Guo, Z. J., 2011, Late Carboniferous collision between the Tarim and Kazakhstan–Yili terranes in the western segment of the South Tian Shan Orogen, Central Asia, and implications for the North Xinjiang, western China: *Earth-Science Reviews*, v. 109, n. 3–4, p. 74–93, <http://dx.doi.org/10.1016/j.earscirev.2011.09.001>
- Han, C. M., Xiao, W. J., Zhao, G. C., Mao, J. W., Li, S. Z., Yan, Z., and Mao, Q. G., 2006, Major types, characteristics and geodynamic mechanism of Upper Paleozoic copper deposits in northern Xinjiang, northwestern China: *Ore Geology Reviews*, v. 28, n. 3, p. 308–328, <http://dx.doi.org/10.1016/j.oregeorev.2005.04.002>
- Hegner, E., Klemm, R., Kröner, A., Corsini, M., Alexeiev, D. V., Iaccheri, L. M., Zack, T., Dulski, P., Xia, X., and Windley, B. F., 2010, Mineral ages and P–T conditions of Late Paleozoic high-pressure eclogite and provenance of mélange sediments from Atbashi in the South Tianshan orogen of Kyrgyzstan: *American Journal of Science*, v. 310, n. 9, p. 916–950, <http://dx.doi.org/10.2475/09.2010.07>
- Heubeck, C., 2001, Assembly of central Asia during the middle and late Paleozoic, in Hendrix, M. S., and Davis, G. A., editors, *Paleozoic and Mesozoic Tectonic Evolution of Central and Eastern Asia: From Continental Assembly to Intracontinental Deformation*: Geological Society of America Memoirs, v. 194, p. 1–22, <http://dx.doi.org/10.1130/0-8137-1194-0.1>
- Jackson, S. E., Pearson, N. J., Griffin, W. L., and Belousova, E. A., 2004, The application of laser ablation-inductively coupled plasma-mass spectrometry to *in-situ* U–Pb zircon geochronology: *Chemical Geology*, v. 211, n. 1–2, p. 47–69, <http://dx.doi.org/10.1016/j.chemgeo.2004.06.017>

- Jahn, B. M., 2004, The Central Asian Orogenic Belt and growth of the continental crust in the Phanerozoic, *in* Malpas, J., Fletcher, C. J. N., and Aitchison, J. C., editors, *Aspects of the Tectonic Evolution of China: The Geological Society, London, Special Publications*, v. 226, p. 73–100, <http://dx.doi.org/10.1144/GSL.SP.2004.226.01.05>
- Jahn, B. M., Wu, F. Y., and Chen, B., 2000a, Granitoids of the Central Asian Orogenic Belt and continental growth in the Phanerozoic: *Transactions of the Royal Society of Edinburgh: Earth Sciences*, v. 91, n. 1–2, p. 181–193, <http://dx.doi.org/10.1017/S0263593300007367>
- 2000b, Massive granitoid generation in Central Asia: Nd isotope evidence and implications for continental growth in the Phanerozoic: *Episodes*, v. 23, p. 82–92.
- Jahn, B. M., Litvinovsky, B. A., Zangvilovich, A. N., and Reichow, M., 2009, Peralkaline granitoid magmatism in the Mongolian–Transbaikalian Belt: Evolution, petrogenesis and tectonic significance: *Lithos*, v. 113, n. 3–4, p. 521–539, <http://dx.doi.org/10.1016/j.lithos.2009.06.015>
- Kröner, A., Windley, B. F., Badarch, G., Tomurtogoo, O., Hegner, E., Jahn, B. M., Gruschka, S., Khain, E. V., Demoux, A., and Wingate, M. T. D., 2007, Accretionary growth and crust formation in the Central Asian Orogenic Belt and comparison with the Arabian–Nubian Shield, *in* Hatcher, R. D., Carlson, M. P., McBride, J. H., and Catalan, J. M., editors, *4-D Framework of the Continental Crust—Integrating Crustal Processes through Time: Geological Society of America Memoirs* 200, p. 181–209, [http://dx.doi.org/10.1130/2007.1200\(11\)](http://dx.doi.org/10.1130/2007.1200(11))
- Kröner, A., Alexeiev, D. V., Rojas-Agramonte, Y., Hegner, E., Wong, J., Xia, X., Belousova, E., Nikolaichuk, A. V., Seltmann, R., Liu, D., and Kiselev, V. V., 2013, Mesoproterozoic (Grenville-age) terranes in the Kyrgyz North Tianshan: Zircon ages and Nd–Hf isotopic constraints on the origin and evolution of basement blocks in the southern Central Asian Orogen: *Gondwana Research*, v. 23, n. 1, p. 272–295, <http://dx.doi.org/10.1016/j.gr.2012.05.004>
- Kröner, A., Kovach, V., Belousova, E., Hegner, E., Armstrong, R., Dolgoplova, A., Seltmann, R., Alexeiev, D. V., Hoffmann, J. E., Wong, J., Sun, M., Cai, K., Wang, T., Tong, Y., Wilde, S. A., Degtyarev, K. E., and Rytisk, E., 2014, Reassessment of continental growth during the accretionary history of the Central Asian Orogenic Belt: *Gondwana Research*, v. 25, n. 1, p. 103–125, <http://dx.doi.org/10.1016/j.gr.2012.12.023>
- Laurent-Charvet, S., Charvet, J., Shu, L. S., Ma, R. S., and Lu, H. F., 2002, Palaeozoic late collisional strike-slip deformations in Tianshan and Altay, eastern Xinjiang, NW China: *Terra Nova*, v. 14, n. 4, p. 249–256, <http://dx.doi.org/10.1046/j.1365-3121.2002.00417.x>
- Laurent-Charvet, S., Charvet, J., Monie, P., and Shu, L. S., 2003, Late Paleozoic strike-slip shear zones in eastern Central Asia (NW China): New structural and geochronological data: *Tectonics*, v. 22, n. 2, p. 1099–1101, <http://dx.doi.org/10.1029/2001TC901047>
- Lees, J., 2002, Three-dimensional anatomy of a geothermal field, Coso, southeast-central California, *in* Glazner, A., Walker, J. D., and Bartley, J. M., editors, *Geologic evolution of the Mojave desert and southwestern basin and range: Geological Society of America Memoirs* 195, p. 259–276, <http://dx.doi.org/10.1130/0-8137-1195-9.259>
- Li, H. Q., Xie, C. F., and Chang, H. L., 1998, Study on metallogenetic chronology of nonferrous and precious metallic ore deposits in North Xinjiang, China: Beijing, Geological Publishing House, p. 62–105 (in Chinese with English abstract).
- Li, J. Y., Wang, K. Z., Li, W. Q., Guo, H. C., Song, B., Wang, Y., Mo, S. G., Zhao, Z. R., Zhu, Z. X., and Pan, C. Z., 2002, Tectonic evolution since the late Paleozoic and mineral prospecting in eastern Tianshan Mountains, NW China: *Xinjiang Geology*, v. 20, p. 295–301 (in Chinese with English abstract).
- Li, J. Y., Wang, K. Z., Sun, G. H., Mo, S. G., Li, W. Q., Yang, T. N., and Gao, L. M., 2006a, Palaeozoic active margin slices in the southern Turfan-Hami basin: geological records of subduction of the Paleo-Asian Ocean plate in central Asian regions: *Acta Petrologica Sinica*, v. 22, n. 5, p. 1087–1102 (in Chinese with English abstract).
- Li, J. Y., Song, B., Wang, K. Z., Li, Y. P., Sun, G. H., and Qi, D. Y., 2006b, Permian mafic-ultramafic complex on the southern margin of the Tu-Ha basins, East Tianshan Mountains: Geological records of vertical crustal growth in Central Asia: *Acta Geologica Sinica*, v. 27, n. 5, p. 424–466 (in Chinese with English abstract).
- Li, S. Z., Ren, Y., Feng, X. C., and Li, S. L., 2006c, Zircon SHRIMP U–Pb dating of granodiorite in the Kizil Tag composite intrusion, south margin of the Tulufan-Hami basin, East Tianshan, Xinjiang, China: With a discussion of the age of emplacement of the intrusion: *Geological Bulletin of China*, v. 25, n. 8, p. 937–940 (in Chinese with English abstract).
- Li, Y. J., Tong, L. L., Du, Z. G., Yang, J. Q., Si, G. H., and Li, X. G., 2007, Geochemical characteristics and tectonic significance of Longdong granitoid rock in Kumutage sandridge area, Eastern Tianshan: *Geological Science and Technology Information*, v. 26, n. 6, p. 25–35 (in Chinese with English abstract).
- Liegeois, J. P., 1998, Preface—Some words on the post-collisional magmatism: *Lithos*, v. 45, p. xv–xvii.
- Litvinovsky, B. A., Tsygankov, A. A., Jahn, B. M., Katzir, Y., and Be'eri-Shlevin, Y., 2011, Origin and evolution of overlapping calc-alkaline and alkaline magmas: The Late Palaeozoic post-collisional igneous province of Transbaikalia (Russia): *Lithos*, v. 125, n. 3–4, p. 845–874, <http://dx.doi.org/10.1016/j.lithos.2011.04.007>
- Ludwig, K. R., 2001, *Squid 1.02: A User Manual*: Berkeley, Berkeley Geochronological Center, Special Publication 2, 19 p.
- Ma, C., Xiao, W. J., Windley, B. F., Zhao, G. P., Han, C. M., Zhang, J. E., Luo, J., and Li, C., 2012, Tracing a subducted ridge–transform system in a late Carboniferous accretionary prism of the southern Altai: Orthogonal sanukitoid dyke swarms in Western Junggar, NW China: *Lithos*, v. 140–141, p. 152–165, <http://dx.doi.org/10.1016/j.lithos.2012.02.005>
- Ma, R. S., Shu, L. S., and Sun, J. Q., 1997, Tectonic evolution and metallogeny of Eastern Tianshan mountains: Beijing, Geological Publishing House, 202 p. (in Chinese with English abstract).

- Mao, J. W., Pirajno, F., Zhang, Z. H., Chai, F. M., Wu, H., Chen, S. P., Cheng, L. S., Yang, J. M., and Zhang, C. Q., 2008, A review of the Cu–Ni sulphide deposits in the Chinese Tianshan and Altay orogens (Xinjiang Autonomous Region, NW China): principal characteristics and ore-forming processes: *Journal of Asian Earth Sciences*, v. 32, n. 2–4, p. 184–203.
- Mao, Q. G., Xiao, W. J., Han, C. M., Sun, M., Yuan, C., Yan, Z., Yong, Y., and Zhang, J. E., 2006, Zircon U–Pb age and the geochemistry of the Baishiquan mafic-ramafic complex in the Eastern Tianshan, Xinjiang province: constraints on the closure of the Paleo-Asian Ocean: *Acta Petrologica Sinica*, v. 22, n. 1, p. 153–162 (in Chinese with English abstract).
- McCulloch, M. T., and Gamble, J. A., 1991, Geochemical and geodynamical constraints on subduction zone magmatism: *Earth and Planetary Science Letters*, v. 102, n. 3–4, p. 358–374, [http://dx.doi.org/10.1016/0012-821X\(91\)90029-H](http://dx.doi.org/10.1016/0012-821X(91)90029-H)
- Metcalf, R. V., and Shervais, J. W., 2008, Supra-subduction zone ophiolites: is there really an ophiolite conundrum? *in* Wright, J. E., and Shervais, J. W., editors, *Ophiolites, Arcs, and Batholiths: Geological Society of America Special Papers*, v. 438, p. 191–222, [http://dx.doi.org/10.1130/2008.2438\(07\)](http://dx.doi.org/10.1130/2008.2438(07))
- Pearce, J. A., 1982, Trace element characteristics of lavas from destructive plate boundaries, *in* Thorp, R. S., editor, *Andesites: Orogenic Andesites and Related Rocks*: New York, John Wiley and Sons, 724 p.
- Pearce, J. A., Harris, N. W., and Tindle, A. G., 1984, Trace element discrimination diagrams for the tectonic interpretation of granitic rocks: *Journal of Petrology*, v. 25, n. 4, p. 956–983, <http://dx.doi.org/10.1093/ptrology/25.4.956>
- Petford, N., 2003, Rheology of granitic magma during ascent and emplacement: *Annual Review of Earth and Planetary Sciences*, v. 31, p. 399–427, <http://dx.doi.org/10.1146/annurev.earth.31.100901.141352>
- Pirajno, F., 2010, Intracontinental strike-slip faults, associated magmatism, mineral systems and mantle dynamics: examples from NW China and Altay-Sayan (Siberia): *Journal of Geodynamics*, v. 50, n. 3–4, p. 325–346, <http://dx.doi.org/10.1016/j.jog.2010.01.018>
- Ren, Y., Guo, H., Tu, Q. J., Feng, X. C., Li, S. Z., and Li, S. L., 2006, Zircon SHRIMP U–Pb of the east Caixiashan quartz diorite stock, south margin of the Tulufan-Hami basin, East Tianshan, Xinjiang, China: *Geological Bulletin of China*, v. 25, n. 8, p. 941–944 (in Chinese with English abstract).
- Sengör, A. M. C., and Natal'in, B. A., 1996, Paleotectonics of Asia: fragments of a synthesis, *in* Yin, A., and Harrison, M., editors, *The Tectonic Evolution of Asia*: Cambridge, Cambridge University Press, p. 486–640.
- Sengör, A. M. C., Natal'in, B. A., and Burtman, V. S., 1993, Evolution of the Altaid tectonic collage and Paleozoic crustal growth in Eurasia: *Nature*, v. 364, p. 299–307, <http://dx.doi.org/10.1038/364299a0>
- Shervais, J. W., 1982, Ti–V plots and the petrogenesis of modern and ophiolitic lavas: *Earth and Planetary Science Letters*, v. 59, n. 1, p. 101–118, [http://dx.doi.org/10.1016/0012-821X\(82\)90120-0](http://dx.doi.org/10.1016/0012-821X(82)90120-0)
- Shi, Y. S., Lu, H. F., Jia, D., and Howell, D. G., 1994, Paleozoic plate tectonic evolution of the Tarim and western Tianshan Regions, Western China: *International Geological Review*, v. 36, n. 11, p. 1058–1066, <http://dx.doi.org/10.1080/00206819409465504>
- Shu, L. S., Charvet, J., Guo, L. Z., Lu, H. F., and Laurent-Charvet, S., 1999, A large-scale Palaeozoic dextral ductile strike-slip zone: the Aqqikkudug-Weiya zone along the northern margin of the Central Tianshan belt, Xinjiang, NW China: *Acta Geologica Sinica*, v. 73, n. 2, p. 148–162.
- Shu, L. S., Chen, Y., Lu, H. F., Charvet, J., Laurent-Charvet, S., and Yin, D. H., 2000, Paleozoic accretionary terranes in Northern Tianshan, NW China: *Chinese Geochemistry*, v. 19, n. 3, p. 193–202, <http://dx.doi.org/10.1007/BF03166877>
- Shu, L. S., Wang, B., Yang, F., Lu, H. F., Charvet, J., and Laurent-Charvet, S., 2003, Polyphase tectonic events and Mesozoic-Cenozoic Basin-Range coupling in the Chinese Tianshan belt: *Acta Geologica Sinica*, v. 77, n. 4, p. 457–467.
- Shu, L. S., Yu, J. H., Charvet, J., Laurent-Charvet, S., Sang, H. Q., and Zhang, R. G., 2004, Geological, geochronological and geochemical features of granulites in the Eastern Tianshan, NW China: *Journal of Asian Earth Sciences*, v. 24, n. 1, p. 25–41, <http://dx.doi.org/10.1016/j.jseae.2003.07.002>
- Shu, L. S., Wang, B., Zhu, W. B., Guo, Z. J., Charvet, J., and Zhang, Y., 2011, Timing of initiation of extension in the Tianshan, based on structural, geochemical and geochronological analyses of bimodal volcanism and olistostrome in the Bogda Shan (NW China): *International Journal of Earth Sciences*, v. 100, n. 7, p. 1647–1663, <http://dx.doi.org/10.1007/s00531-010-0575-5>
- Su, B. X., Qin, K. Z., Sakyi, P. A., Li, X. H., Yang, Y. H., Sun, H., Tang, D. M., Liu, P. P., Xiao, Q. H., and Malaviarachchi, S. P. K., 2011, U–Pb ages and Hf–O isotopes of zircons from Late Paleozoic mafic-ultramafic units in the southern Central Asian Orogenic Belt: Tectonic implications and evidence for an Early-Permian mantle plume: *Gondwana Research*, v. 20, n. 2–3, p. 516–531, <http://dx.doi.org/10.1016/j.jgr.2010.11.015>
- Sun, G. H., Li, J. Y., Wang, D. G., Gao, L. M., and Song, A. J., 2006, Zircon SHRIMP U–Pb ages of granite and granodiorite at the south side of the Aqqikkuduk fault, East Tianshan, Xinjiang, China, and its tectonic implications: *Geological Bulletin of China*, v. 25, n. 8, p. 945–952 (in Chinese with English abstract).
- Sun, S. S., and McDonough, W. F., 1989, Chemical and isotopic systematics of oceanic basalts: implications for mantle composition and processes, *in* Saunders, A. D., and Norry, M. J., editors, *Magmatism in the Ocean Basins: Geological Society, London, Special Publications*, v. 42, p. 313–345, <http://dx.doi.org/10.1144/GSL.SP.1989.042.01.19>
- Tang, G. J., Wang, Q., Wyman, D. A., Li, Z. X., Zhao, Z. H., Jia, X. H., and Jiang, Z. Q., 2010, Ridge subduction and crustal growth in the Central Asian Orogenic Belt: Evidence from Late Carboniferous adakites and high-Mg diorites in the western Junggar region, northern Xinjiang (west China): *Chemical Geology*, v. 277, n. 3–4, p. 281–300, <http://dx.doi.org/10.1016/j.chemgeo.2010.08.012>
- Tang, G. J., Wyman, D. A., Wang, Q., Li, J., Li, Z. X., Zhao, Z. H., and Sun, W. D., 2012a, Asthenosphere–lithosphere interaction triggered by a slab window during ridge subduction: Trace element and Sr–Nd–Hf–Os isotopic evidence from Late Carboniferous tholeiites in the western Junggar area (NW

- China): Earth and Planetary Science Letters, v. 329–330, p. 84–96, <http://dx.doi.org/10.1016/j.epsl.2012.02.009>
- Tang, G. J., Wang, Q., Wyman, D. A., Li, Z. X., Zhao, Z. H., and Yang, Y. H., 2012b, Late Carboniferous high  $\epsilon\text{Nd}(t)$ - $\epsilon\text{Hf}(t)$  granitoids, enclaves and dikes in western Junggar, NW China: Ridge-subduction-related magmatism and crustal growth: *Lithos*, v. 140–141, p. 86–102, <http://dx.doi.org/10.1016/j.lithos.2012.01.025>
- Tang, J. H., Gu, L. X., Zhang, Z. Z., Wu, C. Z., San, J. Z., Wang, C. S., Liu, S. H., and Li, G. R., 2008, Peraluminous granite in Huangshan-Jingerquan area of eastern Tianshan: Geochemistry, mineralogy and geochronology: *Acta Petrologica Sinica*, v. 25, n. 4, p. 921–946 (in Chinese with English abstract).
- Tapponnier, P., and Molnar, P., 1979, Active faulting and Cenozoic tectonics of the Tianshan, Mongolia and Baykal regions: *Journal of Geophysical Research*, v. 84, n. B7, p. 3425–3459, <http://dx.doi.org/10.1029/JB084iB07p03425>
- Vavra, G., Gebauer, D., Schmid, R., and Compston, W., 1996, Multiple zircon growth and recrystallization during polyphase Late Carboniferous to Triassic metamorphism in granulites of the Ivrea Zone (Southern Alps): an ion microprobe (SHRIMP) study: *Contributions to Mineralogy and Petrology*, v. 122, n. 4, p. 337–358, <http://dx.doi.org/10.1007/s004100050132>
- Wang, B., Faure, M., Cluzel, D., Shu, L. S., Charvet, J., and Meffre, S., 2006a, Late Paleozoic tectonic evolution of the northern West Tianshan, NW China: *Geodinamica Acta*, v. 19, n. 3–4, p. 237–247, <http://dx.doi.org/10.3166/ga.19.237-247>
- Wang, B., Chen, Y., Zhan, S., Shu, L. S., Faure, M., Cluzel, D., Charvet, J., and Laurent-Charvet, S., 2007, Primary Carboniferous and Permian paleomagnetic results from Yili Block and their geodynamic implications on evolution of Chinese Tianshan Belt: *Earth and Planetary Science Letters*, v. 263, n. 3–4, p. 288–308, <http://dx.doi.org/10.1016/j.epsl.2007.08.037>
- Wang, B., Faure, M., Shu, L. S., Cluzel, D., Charvet, J., de Jong, K., and Chen, Y., 2008a, Paleozoic tectonic evolution of the Yili Block, western Chinese Tianshan: *Bulletin de la Société Géologique de France*, v. 179, n. 5, p. 483–490, <http://dx.doi.org/10.2113/gssgfbull.179.5.483>
- Wang, B., Cluzel, D., Shu, L. S., Faure, M., Charvet, J., Chen, Y., Meffre, S., and de Jong, K., 2009, Evolution of calc-alkaline to alkaline magmatism through Carboniferous convergence to Permian transcurrent tectonics, western Chinese Tianshan: *International Journal of Earth Sciences*, v. 98, n. 6, p. 1275–1298, <http://dx.doi.org/10.1007/s00531-008-0408-y>
- Wang, B., Faure, M., Shu, L. S., de Jong, K., Charvet, J., Cluzel, D., Jahn, B. M., Chen, Y., and Ruffet, G., 2010, Structural and geochronological study of high-pressure metamorphic rocks in the Kekesu section (northwestern China): implications for the late Paleozoic tectonics of the southern Tianshan: *The Journal of Geology*, v. 118, n. 1, p. 59–77, <http://dx.doi.org/10.1086/648531>
- Wang, B., Shu, L. S., Faure, M., Jahn, B. M., Cluzel, D., Charvet, J., Chung, S. L., and Meffre, S., 2011, Paleozoic tectonics of the southern Chinese Tianshan: insights from structural, chronological and geochemical studies of the Heiyingshan ophiolitic mélange (NW China): *Tectonophysics*, v. 497, n. 1–2, p. 85–104, <http://dx.doi.org/10.1016/j.tecto.2010.11.004>
- Wang, B. Y., Lang, Z., Li, X., Qu, X., Li, T., Huang, C., and Cui, X., 1994, Comprehensive survey of geological sections in the west Tianshan of Xinjiang, China: Beijing, Science Publishing House, 202 p.
- Wang, J. B., Wang, Y. W., and He, Z. J., 2006b, Ore Deposits as a guide to the tectonic evolution in the East Tianshan Mountains, NW China: *Geology in China*, v. 33, n. 3, p. 421–469 (in Chinese with English abstract).
- Wang, L. S., Li, H. Q., Liu, D. Q., and Chen, Y. C., 2005, Geological characteristics and mineralization epoch of Weiquan silver (copper) deposit, Hami, Xinjiang, China: *Mineral Deposits*, v. 24, n. 3, p. 281–284 (in Chinese with English abstract).
- Wang, T., Li, W. P., Li, J. B., Hong, D. W., Tong, Y., and Li, S., 2008b, Increase of juvenile mantle-derived composition from syn-orogenic to post-orogenic granites of the east part of the eastern Tianshan (China) and implication for continental vertical growth: Sr-Nd isotopic evidence: *Acta Petrologica Sinica*, v. 24, n. 4, p. 762–772 (in Chinese with English abstract).
- Wang, Y., Li, J. Y., and Li, W. Q., 2002, Chronological evidence of dextral shear and tectonic evolution of the eastern Tianshan Orogenic Belt: *Xinjiang Geology*, v. 20, n. 4, p. 315–319 (in Chinese with English abstract).
- Wang, Y., Li, J. Y., and Sun, G. H., 2008c, Postcollisional eastward extrusion and tectonic exhumation along the Eastern Tianshan Orogen, Central Asia: Constraints from eextral etrike-elip motion and  $^{40}\text{Ar}/^{39}\text{Ar}$  geochronological evidence: *The Journal of Geology*, v. 116, p. 599–618, <http://dx.doi.org/10.1086/591993>
- Weinberg, R. F., Sial, A. N., and Mariano, G., 2004, Close spatial relationship between plutons and shear zones: *Geology*, v. 32, n. 5, p. 377–380, <http://dx.doi.org/10.1130/G20290.1>
- Wilson, M., 1989, Igneous petrogenesis: A global tectonic approach: London, Unwin Hyman, 480 p.
- Windley, B. F., Alexiev, D., Xiao, W. J., Kröner, A., and Badarch, G., 2007, Tectonic models for accretion of the Central Asian Orogenic belt: *Journal of the Geological Society*, v. 164, n. 1, p. 31–47, <http://dx.doi.org/10.1144/0016-76492006-022>
- Wu, C. W., Liao, Q. A., Li, Q. X., and Yang, Z. F., 2008, The late Carboniferous volcanic arc rocks in Jueluotage area, Eastern Tianshan, China: *Geological Science and Technology Information*, v. 27, p. 29–36 (in Chinese with English abstract).
- Xia, L. Q., Xu, X. Y., Xia, Z. C., Li, X. M., Ma, Z. P., and Wang, L. S., 2004, Petrogenesis of Carboniferous rift-related volcanic rocks in the Tianshan, northwestern China: *Geological Society of America Bulletin*, v. 116, n. 3–4, p. 419–433, <http://dx.doi.org/10.1130/B25243.1>
- Xia, L. Q., Xia, Z. C., Xu, X. Y., Li, X. M., and Ma, Z. P., 2008, Relative contributions of crust and mantle to the generation of the Tianshan Carboniferous rift-related basic lavas, northwestern China: *Journal of Asian Earth Sciences*, v. 31, n. 4–6, p. 357–378, <http://dx.doi.org/10.1016/j.jseas.2007.07.002>

- Xiao, Q. H., Qin, K. Z., Tang, D. M., Su, B. X., Sun, H., San, J. Z., Cao, M. J., and Hui, W. D., 2010b, Xiangshanxi composite Cu-Ni—Ti-Fe deposit belongs to comagmatic evolution product: Evidences from ore microscopy, zircon U-Pb chronology and petrological geochemistry, Hami, Xinjiang, NW China: *Acta Petrologica Sinica*, v. 26, n. 2, p. 503–522 (in Chinese with English abstract).
- Xiao, W. J., Zhang, L. C., Qin, K. Z., Sun, S., and Li, J. L., 2004, Paleozoic accretionary and collisional tectonics of the eastern Tianshan (China): Implications for the continental growth of Central Asia: *American Journal of Science*, v. 304, n. 4, p. 370–395, <http://dx.doi.org/10.2475/ajs.304.4.370>
- Xiao, W. J., Kröner, A., and Windley, B. F., 2009a, Geodynamic evolution of Central Asia in the Paleozoic and Mesozoic: *International Journal of Earth Sciences*, v. 98, n. 6, p. 1185–1188, <http://dx.doi.org/10.1007/s00531-009-0418-4>
- Xiao, W. J., Windley, B. F., Yuan, C., Sun, M., Han, C. M., Lin, S. F., Chen, H. L., Yan, Q. R., Liu, D. Y., Qin, K. Z., Li, J. L., and Sun, S., 2009b, Paleozoic multiple subduction-accretion processes of the southern Altai: *American Journal of Science* v. 309, n. 3, p. 221–270, <http://dx.doi.org/10.2475/03.2009.02>
- Xiao, W. J., Huang, B. C., Han, C. M., Sun, S., and Li, J. L., 2010a, A review of the western part of the Altai: A key to understanding the architecture of accretionary orogens: *Gondwana Research*, v. 18, n. 2–3, p. 253–273, <http://dx.doi.org/10.1016/j.gr.2010.01.007>
- Xiao, X. C., Tang, Y. Q., Feng, Y. M., Zhu, B. Q., Li, J. Y., and Zhao, M., 1992, Tectonic evolution of the northern Xinjiang and its adjacent regions: Beijing, Geology Publishing House, p. 12–47 (in Chinese with English abstract).
- XJBGM (Xinjiang Bureau of Geology and Mineral Resources), 1993, Regional geology of Xinjiang Uygur Autonomous Region: Beijing, Geological Publishing House, 376 p. (in Chinese with English abstract).
- Xu, X. W., Ma, T. L., Sun, L. Q., and Cai, X. P., 2003, Characteristics and dynamic origin of the large-scale Jiaoutage ductile compressional zone in the eastern Tianshan Mountains, China: *Journal of Structural Geology*, v. 25, n. 11, p. 1901–1915, [http://dx.doi.org/10.1016/S0191-8141\(03\)00017-8](http://dx.doi.org/10.1016/S0191-8141(03)00017-8)
- Yang, H., ms, 1998, Genesis, Characteristics, distribution rules of granite in the eastern Tianshan Mountain and its relationship to tectonics setting and ore deposit: Nanjing, China, Nanjing University, M. S. thesis, 80 p.
- Yin, A., and Nie, S. Y., 1996, A Phanerozoic palinspastic reconstruction of China and its neighboring regions, in Yin, A., and Harrison, M., editors, *The Tectonic Evolution of Asia*: Cambridge, Cambridge University Press, Rubey Colloquium, p. 442–485.
- Zhang, D. Y., Zhang, Z. C., Encarnación, J., Xue, C. J., Duan, S. G., Zhao, Z. D., and Liu, J. L., 2012, Petrogenesis of the Kekesai composite intrusion, western Tianshan, NW China: Implications for tectonic evolution during late Paleozoic time: *Lithos*, v. 146–147, p. 65–79, <http://dx.doi.org/10.1016/j.lithos.2012.04.002>
- Zhang, H. R., Wei, G. F., Li, Y. J., Du, Z. G., and Chai, D. L., 2010, Carboniferous lithologic association and tectonic evolution of Dananhu arc in the East Tianshan Mountains: *Acta Petrologica et Mineralogica*, v. 29, p. 1–14 (in Chinese with English abstract).
- Zhang, L. F., Ai, Y. L., Li, X. P., Rubatto, D., Song, B., Williams, S., Song, S. G., Ellis, D. J., and Liou, J. G., 2007, Triassic collision of western Tianshan orogenic belt, China: Evidence from SHRIMP U-Pb dating of zircon from HP/UHP eclogitic rocks: *Lithos*, v. 96, n. 1–2, p. 266–280, <http://dx.doi.org/10.1016/j.lithos.2006.09.012>
- Zhang, X. M., Wang, D. G., and Li, G., 2006, SHRIMP U-Pb dating of zircon from the east Shalong monzogranite in Kumtag, East Tianshan, Xinjiang, China: *Geological Bulletin of China*, v. 25, n. 8, p. 957–959 (in Chinese with English abstract).
- Zhou, M. F., Leshner, C. M., Yang, Z. X., Li, J. W., and Sun, M., 2004, Geochemistry and petrogenesis of 270 Ma Ni–Cu-(PGE) sulfide-bearing mafic intrusions in the Huangshan district, Eastern Xinjiang, Northwest China: implications for the tectonic evolution of the Central Asian orogenic belt: *Chemical Geology*, v. 209, n. 3–4, p. 233–257, <http://dx.doi.org/10.1016/j.chemgeo.2004.05.005>
- Zhou, M. F., Zhao, J. H., Jiang, C. Y., Gao, J. F., Wang, W., and Yang, S. H., 2009, OIB-like, heterogeneous mantle sources of Permian basaltic magmatism in the western Tarim Basin, NW China: implications for a possible Permian large igneous province: *Lithos*, v. 113, n. 3–4, p. 583–594, <http://dx.doi.org/10.1016/j.lithos.2009.06.027>
- Zhou, T. F., Yuan, F., Zhang, D. Y., Fan, Y., Liu, S., Peng, M. X., and Zhang, J. D., 2010, Geochronology, tectonic setting and mineralization of granitoids in Jueluotage area, eastern Tianshan, Xinjiang: *Acta Petrologica Sinica*, v. 26, n. 2, p. 478–502 (in Chinese with English abstract).